

Topical Review

Progress of hydrogenation engineering in crystalline silicon solar cells: a review

Lihui Song^{1,2,3,*} , Zechen Hu^{1,3} , Dehang Lin¹, Deren Yang^{1,2} and Xuegong Yu^{1,*} 

¹ State Key Laboratory of Silicon Materials and Department of Materials Science and Engineering, Zhejiang University, No.38 Zheda Road, Hangzhou 310027, People's Republic of China

² Institute of Advanced Semiconductors & Zhejiang Provincial Key Laboratory of Power Semiconductor Materials and Devices, ZJU-Hangzhou Global Scientific and Technological Innovation Center, Zhejiang University, Hangzhou 311200, People's Republic of China

E-mail: songlihui@zju.edu.cn and yuxuegong@zju.edu.cn

Received 16 February 2022, revised 18 June 2022

Accepted for publication 8 September 2022

Published 22 September 2022



Abstract

Crystalline silicon solar cells are always moving towards 'high efficiency and low cost', which requires continuously improving the quality of crystalline silicon materials. Nevertheless, crystalline silicon materials typically contain various kinds of impurities and defects, which act as carrier recombination centers. Therefore these impurities and defects must be well controlled during the solar cell fabrication processes to improve the cell efficiency. Hydrogenation of crystalline silicon is one important method to deactivate these impurities and defects, which is so-called 'hydrogenation engineering' in this paper. Hydrogen is widely reported to be able to passivate diverse defects like crystallographic defects, metallic impurities, boron–oxygen related defects and etc, but the effectiveness of hydrogen passivation depends strongly on the processing conditions. Moreover, in this decade, advanced hydrogenation technique has been developed and widely applied in the photovoltaic industry to significantly improve the performance of silicon solar cells. As the research on hydrogenation study has made a significant progress, it is the right time to write a review paper on introducing the state-of-the-art hydrogenation study and its applications in photovoltaic industry. The paper first introduces the fundamental properties of hydrogen in crystalline silicon and then discusses the applications of hydrogen on deactivating/inducing typical defects (e.g. dislocations, grain boundaries, various metallic impurities, boron–oxygen related defects and light and elevated temperature induced degradation defect) in p- and n-type crystalline silicon, respectively. At last, the benefits of hydrogenation engineering on the next-generation silicon solar cells (e.g. tunnel oxide passivated contact (TOPCon) and silicon heterojunction (SHJ) solar cells) are discussed. Overall, it was found that hydrogen can deactivate most of typical defects (sometimes induce defect) in n- and p-type crystalline silicon, leading to a significant efficiency enhancement in passivated emitter rear contact, TOPCon and SHJ solar cells. In conclusion, the paper aims to assist young researchers to better understand hydrogenation research.

Keywords: crystalline silicon, hydrogenation, crystallographic defects, boron–oxygen related defects, LeTID

(Some figures may appear in colour only in the online journal)

³ The authors contributed equally to this work.

* Authors to whom any correspondence should be addressed.

1. Introduction

Crystalline silicon solar cells always move towards ‘high efficiency and low cost’. To achieve this goal, some new device architectures of silicon solar cells were invented to pursue high efficiency, including passivated emitter rear contact (PERC), tunnel oxide passivated contact (TOPCon), silicon heterojunction (SHJ), interdigitated back contact solar cells [1–4]. These high efficiency cell architectures typically require high quality crystalline silicon wafers to obtain a high bulk lifetime. However, high quality silicon wafers are very expensive and hence are typically not adopted by photovoltaic industry from the viewpoint of cost. Therefore, a good passivation of low cost silicon wafers becomes of great importance to the photovoltaic industry. Nevertheless, low cost silicon wafers suffer from various kinds of defects, like grain boundary (GB), dislocation, metallic impurities, boron–oxygen (B–O) related defects, light and elevated temperature induced degradation (LeTID) defect and etc. Hydrogenation is an effective method to passivate most of defects in crystalline silicon, and thus becomes an important technique to improve cell efficiency in photovoltaic industry [5, 6]. Nevertheless, hydrogenation technique is a complex research, its mechanisms and effectiveness depends on many factors such as the defect type, excess carrier concentration and etc, and therefore it is crucial to introduce hydrogenation study via differentiating the different categories of the defect types. Moreover, recent research on hydrogenation carefully studies the manipulation of charge states of hydrogen on passivating various kinds of defects, and many interesting results emerged associated with the better cell performance. To give an overview on hydrogenation research, we will first introduce the fundamental properties of hydrogen in crystalline silicon, and then the applications of hydrogenation on deactivating/inducing various kinds of defects, and finally the benefits of hydrogenation on next-generation crystalline silicon solar cells.

To understand hydrogenation, it is essential to introduce the fundamental properties of hydrogen in crystalline silicon, which includes the introduction of hydrogen solubility, diffusivity, charge states, energy levels in bandgap and the hydrogen source. Here a brief outlook of the fundamental properties of hydrogen in crystalline silicon is summarized. To begin with, the solubility of hydrogen in crystalline silicon heavily depends on temperature. For instance, Binns *et al* [7] claimed an expression for hydrogen solubility in crystalline silicon for the temperature ranging from 900 °C to 1300 °C, finding that the solubility of hydrogen increases exponentially with the temperature in the given temperature range. For the general concern, the solubility of hydrogen in crystalline silicon at room temperature is found to be around 10^{16} atoms cm^{-3} as reported in [8]. In addition, the solubility of hydrogen is found to increase with the concentration of crystallographic defects in crystalline silicon [9], and therefore multi-crystalline silicon typically can incorporate more interstitial hydrogen in silicon bulk. For hydrogen diffusivity, the diffusivity of hydrogen depends on many factors like temperature, dopant type and concentration, internal/external electric field and etc. When temperature is above 700 °C, hydrogen diffuses very fast and

dominantly in the form of interstitial hydrogen [10, 11]. When temperature is modest (e.g. between 200 °C and 700 °C), the hydrogen diffusivity is dramatically reduced due to its interactions with dopants and impurities [12, 13], however, in this case hydrogen still diffuses dominantly in the form of interstitial hydrogen. Nevertheless, when temperature is below 200 °C, hydrogen mainly diffuses in the form of hydrogen dimers and its diffusivity is determined by the diffusivity of hydrogen dimers in crystalline silicon, which is typically very slow. For hydrogen charge state, it is another important property of atomic hydrogen, as it can significantly influence the interstitial hydrogen’s diffusivity and reactivity. In detail, Johnson *et al* [14] first reported that interstitial hydrogen occupies three charge states in crystalline silicon, namely H^+ (positively charged), H^- (negatively charged) and H^0 (neutral). Besides, the fractional concentrations of H^+ , H^- and H^0 vary with the position of Fermi level in silicon bandgap [15]. For instance, the majority of interstitial hydrogen is H^+ in p-type silicon due to the abundant of holes, whereas the majority of interstitial hydrogen is H^- in n-type silicon. Manipulation of hydrogen charge states can have significant impacts on their diffusivity and electronic properties. For example, Kamiura *et al* [16] reported an enhanced diffusivity of H^0 over H^+ and H^- about five orders of magnitude at 423 K. In terms of the reactivity, Liu *et al* [17] reported an enhanced passivation of interstitial iron in silicon by taking advantage of H^0 or H^- . Moreover, Hallam *et al* [18] reported the accelerated passivation of B–O related defects via laser changing the hydrogen charge state to H^0 or H^- . The energy levels of interstitial hydrogen in crystalline silicon are reported by Herring *et al* [15], which lie at E_c (conduction band)—0.16 eV for donor level and E_i (middle bandgap)—0.07 eV for acceptor level. These two energy levels indicate that interstitial hydrogen processes a negative U property in concentration [19], which suggests that H^0 can never be a dominant hydrogen species. For the hydrogen source in crystalline silicon, it can typically be the hydrogenated silicon nitride, hydrogen plasma, hydrogen forming gas and etc. Nevertheless, for the commercial applications, the hydrogenated silicon nitride is widely adopted as the hydrogen source. Generally, the hydrogen content in the hydrogenated silicon nitride is modulated by varying the refractive index of the film, which changes the concentrations of Si–H and N–H bonds in the film. In summary, understanding the fundamental properties of hydrogen in crystalline silicon is crucial and more details are provided in section 2.

Hydrogenation has wide applications in deactivating/pasivating various kinds of defects in crystalline silicon. One of these applications is the hydrogen deactivation of dopants in crystalline silicon. So far, hydrogen was reported to be able to deactivate boron and phosphorus [20], leading to the reduced effective doping of crystalline silicon. Crystallographic defects are another type of defects that can be deactivated by hydrogen. Hydrogenation of dislocation is widely reported and its effectiveness depends on the dislocation type, the contamination level and the processing conditions. For instance, Martinuzzi *et al* [21] found that the dislocation in crystalline silicon exhibits two kinds of defect energy levels, namely deep defect energy level and shallow defect energy

level. The deep defect energy level is associated with the dislocation part decorated with metallic impurity and the shallow defect energy level is associated with the dislocation part with little impurity contamination. It is found that the shallow defect energy level can be completely passivated by hydrogen, whereas the deep defect energy level is transformed into the shallow energy level by hydrogenation. Moreover, Ciesla *et al* [22] reported that hydrogen charge state manipulation can enhance the passivation effectiveness of dislocation by interstitial hydrogen. In detail, they compared the impact of illuminated annealing and dark annealing on dislocation passivation, and found that illuminated annealing can increase the passivation extent of dislocation in cast mono-like silicon, which is due to that illuminated annealing changes the charge state of interstitial hydrogen into H^0 and H^- . GB is another typical type of crystallographic defects that can be passivated by hydrogen. It is found that the passivation effectiveness of GB by hydrogen strongly depends on the GB character and the contamination level. For instance, Bardhadi *et al* [23] reported that hydrogen is more effective for the passivation of small angle GB as compared to large angle GB, as large angle GB typically has a strong ability to getter impurities into it. In terms of contamination level, GB passivation by hydrogen is normally more effective for clean GB as compared to the contaminated counterpart. It was demonstrated by Park *et al* [24] that hydrogenation can decrease the density of dangling bonds in clean GB by a factor of between three and an order of magnitude. In contrast, hydrogenation on GB decorated with metallic impurity was much weaker as reported by Jiang *et al* [25]. It was found that the density of the contaminated GB states varied only slightly after hydrogenation. Hydrogenation is also able to passivate various kinds of metal impurities in crystalline silicon. For instance, Jones *et al* [26] reported hydrogenation of nickel impurity in crystalline silicon. Moreover, Cu, Ag, Au and Pt are reported to be effectively passivated by interstitial hydrogen [27]. Recently, it was found that hydrogen plays an important role on the permanent deactivation of B–O related defects. In detail, Nampalli *et al* [28] experimentally confirmed that the permanent deactivation of B–O related defects can only occur with the presence of hydrogen in silicon bulk. Furthermore, Wilking *et al* [29] reported that uncharged H^0 is directly responsible for the permanent passivation of B–O related defects and therefore the regeneration rate is dependent on the concentration of uncharged H^0 rather than the total concentration of monatomic hydrogen in silicon. Hydrogen can not only passivate defects, but also can induce defects in crystalline silicon. Recently, it was widely reported that hydrogen is responsible for the formation and activation of LeTID defect in crystalline silicon [30]. Except for LeTID defect, Hamer *et al* [31] demonstrated that hydrogen can deactivate the phosphorus atoms or counter-dope in the contact region to increase the contact resistance of the electrode when multi-crystalline silicon solar cells were subject to a post-firing annealing. In summary, hydrogenation finds huge applications in deactivating/passivating diverse defects in crystalline silicon and more details are provided in section 3.

Hydrogenation is vital not only due to the ability of hydrogen to passivate almost all of typical defects in crystalline silicon, but also due to the ability of hydrogenation to significantly improve the efficiency and the open circuit voltage of the commercial solar cells (e.g. PERC) and the next-generation solar cells (e.g. TOPCon and SHJ). It was demonstrated by Ciesla *et al* [32] that a hydrogenation process applied at the step of metal sintering was able to enhance the efficiency of PERC solar cells by more than 0.2% absolute. Furthermore, Liu *et al* [33] modified the refractive index of hydrogen containing films to enhance the hydrogen in-diffusion to the silicon bulk, which enables a high efficiency of 23.22% achieved on n-type cast-mono silicon PERC solar cells. For the next-generation n-type TOPCon or SHJ solar cells, the efficiency enhancement by hydrogenation is more significant. For example, Madumelu *et al* [34] reported that an illuminated annealing process, which should induce enhanced hydrogenation of silicon surface, could enhance the efficiency of SHJ solar cells by more than 0.2% absolute. Furthermore, according to the authors' experimental results, a post-firing hydrogenation step achieved by current injection at low temperature can enhance the efficiency of TOPCon solar cells by 0.4% absolute, which will be published in another paper soon. Wright *et al* [35, 36] also summarized the recent studies on hydrogenation application in SHJ solar cells in a recent review paper, which demonstrated that appropriate surface passivation improvement by hydrogen combined with the optimization of carrier transport in n-type silicon can enhance efficiency by 0.7% absolute. In summary, hydrogenation is vital for the conventional and the next generation silicon solar cells due to its strong ability to enhance their efficiency. More details on hydrogenation applications are provided in section 4.

2. Fundamental properties of hydrogen in crystalline silicon

2.1. Diverse forms of hydrogen

After the introduction of hydrogen into the crystalline silicon, hydrogen can exist in several forms, including hydrogen plateau, hydrogen dimer, interstitial hydrogen and hydrogen bound state. First of all, interstitial hydrogen is an important form of hydrogen in crystalline silicon, as it is chemically active to passivate various kinds of defects. At high temperatures above 900 °C, almost all the hydrogen is in the form of interstitial hydrogen. Nevertheless, the fraction of interstitial hydrogen decreases rapidly with the decreased temperature. When the temperature is below 100 °C, interstitial hydrogen only accounts for a small fraction of total hydrogen concentration, as most of interstitial hydrogen will bond to dopants/defects or form dimers. As interstitial hydrogen is chemically active, it is crucial to make full use of interstitial hydrogen to passivate diverse defects. In this decade, a newly developed advanced hydrogenation technique takes advantage of interstitial hydrogen charge state control to improve hydrogenation performance, as certain charged defects typically require negatively

charged hydrogen to passivate. More information on hydrogen charge state can be found in section 2.2.

Second, hydrogen can be in a bound state, for instance bound to dopants, or metallic impurities, or silicon dangling bonds. Hydrogen-dopant complex is widely reported and studied, which are typically H–B and H–P complexes in conventional silicon solar cells. Recent study [37] suggested that H–Ga complex also existed in gallium doped crystalline silicon and had a higher formation energy as compared to H–B complex. More details of hydrogen-dopant complex are in section 3.1. In addition, the hydrogen-metallic impurity complexes are widely reported including H–Fe complex, H–Pt complex, H–Ti complex, H–V complex, H–Cr complex and etc. More details about H-metallic impurity complexes are in section 3.2. H-dangling bond complex is very common in crystalline silicon, it exists in the hydrogen passivated silicon surface, dislocation and GB [38]. H-dangling bond complex is typically very stable against the illumination and the modest temperature, but carrier injection is able to lower its binding energy. More details on H-dangling bond complex can be found in sections 3.3–3.5.

Third, hydrogen is able to form dimers in crystalline silicon. In a recent paper, Voronkov *et al* [39] found that there exists three kinds of hydrogen dimers in crystalline silicon after the co-firing process, which is named as H_{2A} (one metastable hydrogen dimer structure), H_{2B} (one stable hydrogen dimer structure) and H_{2C} (another metastable hydrogen dimer structure) [15], respectively. Just after firing the hydrogenated silicon nitride film, H_{2A} dominates the total hydrogen concentration, however, it will convert to H–B complex under dark annealing at the moderate temperatures (100 °C–350 °C). H_{2B} is a metastable dimer with a high diffusivity created by quenching. Up to date, the pairing reaction of H_{2B} cannot be specified yet, but most likely it involves a reaction of atomic hydrogen with H–B complex. H_{2C} is a stable dimer with a low diffusivity that is created during the exposure to a plasma, then in-diffuses from the surface, and also can be generated in the sample bulk. Furthermore, H_{2C} can be produced by annealing samples quenched from high T. The pairing reaction to create H_{2C} is most likely $H^+ + HB \rightarrow H_{2C} + B^- + 2 h^+$. The conversion of H–B complex to H_{2A} and H_{2C} dimers by annealing can somewhat be seen via figure 1. By the way, the authors hypothesized that H_{2A} and H_{2C} might play an important role on the kinetics of LeTID reaction, which will be discussed in section 3.6.

Fourth, hydrogen is able to form platelets at the silicon surface when silicon sample is processed with hydrogen plasma treatment. In the literature, Nickel *et al* [40] found that hydrogen induced platelets can only form for the Fermi-level positions of $E_C - E_F < 0.3$ eV and confirmed that the formation of hydrogen-induced platelets is solely controlled by the Fermi energy, as shown in figure 2. In terms of the mechanism, the authors claimed that the nucleation of hydrogen-induced platelets requires positively (H^+) and negatively charged hydrogen (H^-) atoms, and therefore platelets can nucleate and grow only when the Fermi energy is equal to the mean value of the hydrogen donor and acceptor levels. In addition, the microscopic structure of hydrogen-induced platelets is still unknown

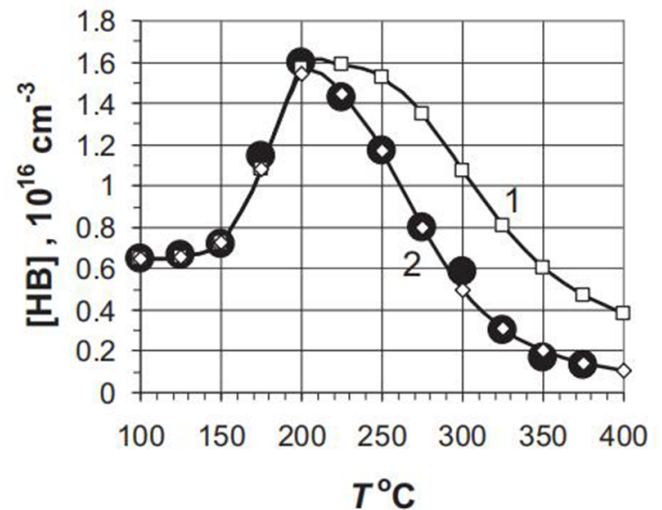


Figure 1. Variation in the concentration of HB by isochronal anneal for 30 min with a step of 25 °C. The boron concentration $N_B = 10^{17} \times \text{cm}^{-3}$, the total hydrogen concentration $C_{\text{tot}} = 1.6 \times 10^{16} \text{ cm}^{-3}$. The simulated curve 1 is for the HB + H_{2A} subsystem, and the curve 2 is for HB + H_{2A} + H_{2C} system. [40] John Wiley & Sons. © 2017 WILEY-VCH Verlag GmbH & Co. KGaA, Weinheim.

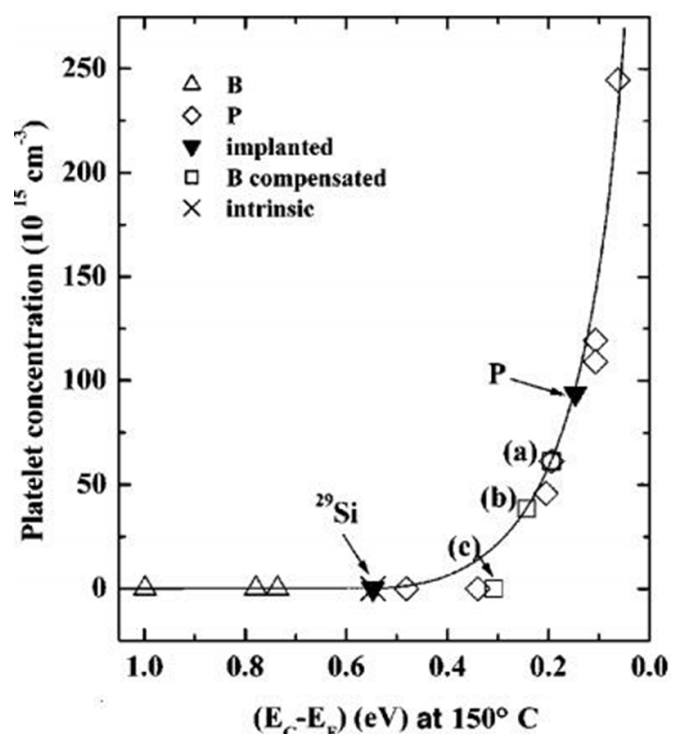


Figure 2. Platelet concentration in crystalline silicon (c-Si) as a function of the Fermi energy ($E_C - E_F$) at 150 °C. Reprinted (figure) with permission from [42], Copyright (2000) by the American Physical Society.

according to the literature. Nevertheless, it is worth noting that hydrogen introduced from the hydrogenated silicon nitride film through the well-known co-firing step is as well able to induce platelets underneath the silicon surface [42].

In summary, hydrogen can exist in several forms in crystalline silicon, including hydrogen platelet, hydrogen dimer, interstitial hydrogen and hydrogen bound state. Different forms of hydrogen have distinct electrical properties and may interact with different defects. For hydrogenation, interstitial hydrogen is the most significant as it is chemically active to passivate defects. Other forms of hydrogen are important as well since they can influence the effectiveness of hydrogenation.

2.2. Charge states of interstitial hydrogen

Interstitial hydrogen is significant to hydrogenation as it is chemically active to passivate diverse defects. Studies by Herring *et al* [15] pointed out that interstitial hydrogen has three charge states, namely H^+ (positively charged), H^- (negatively charged) and H^0 (neutral). These three charge states of hydrogen (briefed as hydrogen for interstitial hydrogen in the later part) have distinct configurations and electrical properties in crystalline silicon. Typically, H^+ possesses the bond center position, midway between two silicon atoms. Whereas H^- possesses the interstitial position of tetrahedral site. For H^0 , it has two possible positions at the bond center position or at the interstitial position of tetrahedral site, which corresponds to the H^0 transformed from H^+ and H^- , respectively. Hydrogen can introduce two energy levels in silicon bandgap, of which one is a donor level positioned at $E_c - 0.16$ eV [15] and another one is an acceptor level positioned at $E_v + 0.48$ eV [15], as shown in equations (1) and (2):

$$E_D = E_C - 0.16 \text{ eV} \quad (1)$$

$$E_A = E_V + 0.48 \text{ eV}. \quad (2)$$

As the donor level of hydrogen is above the acceptor level of hydrogen in silicon bandgap, hydrogen is an impurity with negative-U property, which means that H^0 can never be a dominant hydrogen specie. Deriving from the energy levels of hydrogen, the fractional concentrations of various hydrogen charge states as a function of the Fermi energy can be illustrated by figure 3 in the condition of thermal equilibrium. As seen in figure 3, the minority charge states of hydrogen (for instance H^0 and H^- in p-type silicon) are typically in very low concentration in conventional p-type and n-type silicon wafers at room temperature. Nevertheless, carrier injection is able to enhance the fractional concentration of the minority hydrogen charge state significantly, and hence improve the effectiveness of hydrogenation. For example, Sun *et al* [42] studied the impacts of carrier injection on the concentration of H^0 via using the model of Sah-Shockley statistics, which can be well revealed by figure 4. In their paper, the concentration of H^0 is positively correlated with the performance of hydrogenation. More details on hydrogen charge state modulation can be found in the review paper by Hallam *et al* [43].

It is worth noting that manipulation of hydrogen charge state plays a significant role on enhancing the effectiveness of defect passivation. For instance, as mentioned in the introduction, H^0 has the faster diffusivity about five orders of

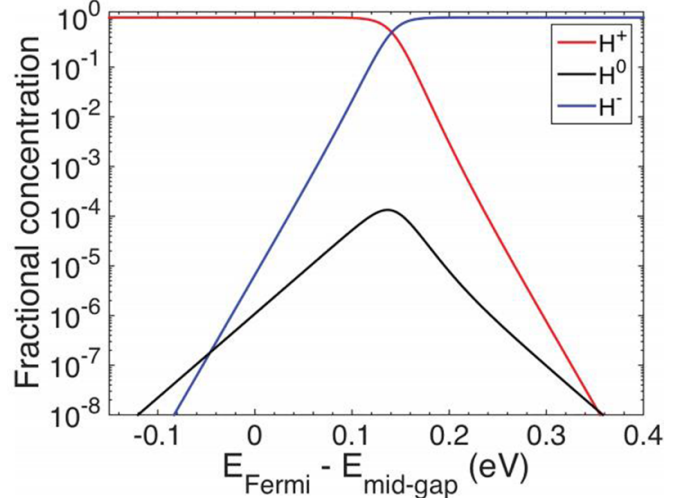


Figure 3. Fractional hydrogen charge state concentrations of interstitial hydrogen in silicon in thermal equilibrium at room temperature as a function of the Fermi level (E_{Fermi}) relative to the midgap energy level ($E_{\text{mid-gap}}$). Reproduced from [37]. CC BY 4.0.

magnitude over H^- and H^+ at 423 K, and therefore can be vital in passivating defects during the fast-firing process. In terms of the reactivity, Liu *et al* [14] reported that the hydrogenation of interstitial iron in crystalline silicon can be dramatically enhanced by taking advantage of H^- and H^0 . Furthermore, Hallam *et al* [44] successfully used laser to enhance the concentration of H^0 to accelerate the regeneration rate of B–O related defects. More applications of hydrogen charge state control on improving defect passivation can be found in sections 3.1–3.6.

In summary, hydrogen has three charge states in crystalline silicon, namely H^+ , H^- and H^0 . The fractional concentration of these three charge states depends on the position of Fermi level in silicon bandgap. As the Fermi level approaches to the conduction band, the H^- dominates over all the interstitial hydrogen. Whereas the Fermi level approaches to the valence band, the H^+ dominates. Hydrogen can introduce two energy levels in silicon bandgap at $E_c - 0.16$ eV (donor level) and $E_v + 0.48$ eV (acceptor level). As the donor level of hydrogen is above the acceptor level, hydrogen is a negative-U impurity, which means that H^0 can never be a dominant hydrogen specie. In addition, hydrogen charge states play an important role on hydrogen electrical properties. Recent works demonstrated that manipulation of hydrogen charge states can significantly improve the hydrogenation performance.

2.3. Solubility of hydrogen in silicon

The solubility of hydrogen typically refers to the solubility of interstitial hydrogen in crystalline silicon. Hydrogen (refers to interstitial hydrogen in this section) can dissolve in crystalline silicon as isolated hydrogen atom and its solubility strongly depends on temperature. For instance, McQuaid *et al* [45] reported that the solubility of hydrogen at 1300 °C was $1.5 \times 10^{16} \text{ cm}^{-3}$. Binns *et al* [7] further extended the data

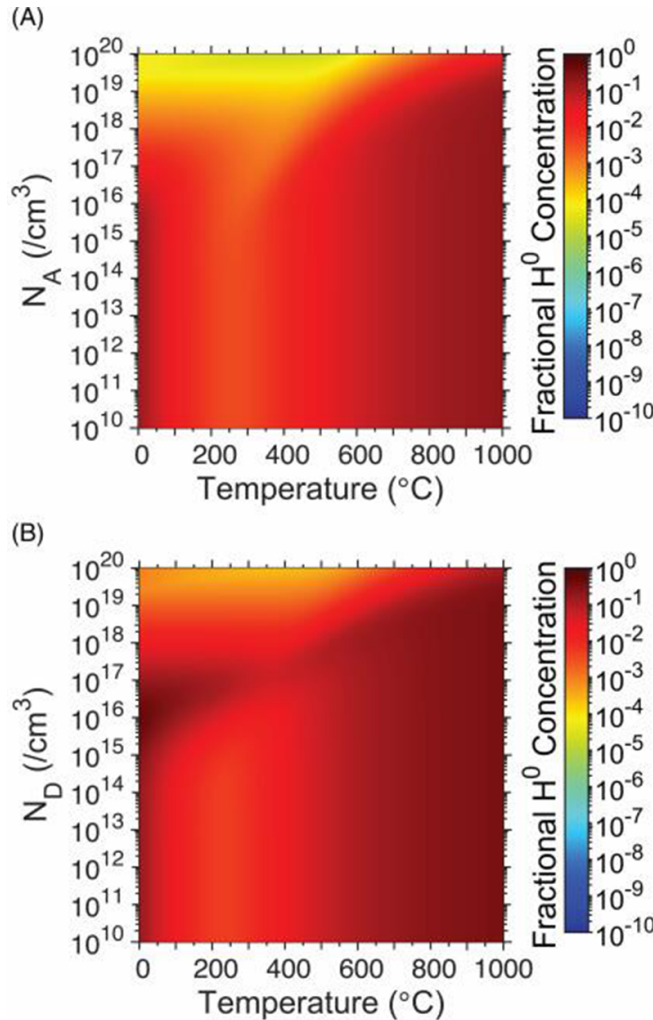


Figure 4. Fractional H^0 concentrations in $1\ \Omega\cdot\text{cm}$ silicon material as a function of temperature and doping concentration for (A) p-type silicon (N_A , acceptor concentration) and (B) n-type silicon (N_D , donor concentration) using Sah-Shockley occupation statistics. Reproduced from [37]. CC BY 4.0.

for the temperatures ranging from $900\ ^\circ\text{C}$ to $1300\ ^\circ\text{C}$, as expressed in equation (3):

$$[H_s] = 9.1 \times 10^{21} \exp(-1.80 \text{ eV kT}^{-1}) \text{ cm}^{-3} \quad (3)$$

From equation (3), the extracted solubility of hydrogen in silicon at $1300\ ^\circ\text{C}$ is $1.58 \times 10^{16}\ \text{cm}^{-3}$, which is in agreement with the [45]. It is evident that the solubility of hydrogen reduces with the decreased temperature, and when the temperature is $900\ ^\circ\text{C}$, the solubility of hydrogen in crystalline silicon is only $1.72 \times 10^{14}\ \text{cm}^{-3}$. For the temperatures below $900\ ^\circ\text{C}$, it can be expected that the solubility of hydrogen will continuously decrease with the reducing temperature. Nevertheless, as far as the authors know, no hydrogen solubility data at low temperature is reported in the literature, possibly due to the detection limit of the characterization tools. However, it can be speculated that the solubility of hydrogen at low temperatures should be significantly below the trend of the equation (3) due to the interactions of hydrogen with dopants. In addition, some researchers [9] reported that surface damage due to plasma

exposure can improve the solubility of hydrogen in crystalline silicon, as voids in the surface damage layer provide the space for hydrogen to accumulate. Nevertheless, it is worth noting that the accumulated hydrogen in voids is not necessarily to be the dissolved hydrogen and can be the hydrogen dimers and so on.

In summary, the solubility of hydrogen in crystalline silicon depends on temperature, the interaction with dopants, the void concentration and etc. At high temperatures above $900\ ^\circ\text{C}$, the solubility of hydrogen follows equation (3). However, at low temperatures below $900\ ^\circ\text{C}$, the solubility of hydrogen should be below the above trend due to the interaction with dopants.

2.4. Diffusivity of hydrogen

The diffusivity of hydrogen in crystalline silicon was extensively studied by researchers. Wieringen *et al* [8] first derived the hydrogen diffusivity at high temperatures ranging from 1243 to 1473 K, as expressed in equation (4). At such high temperatures, hydrogen dominantly exist in the form of interstitial hydrogen, and hence this extracted diffusivity data is typically considered as the upper limit for hydrogen diffusivity:

$$D_H = 9.4 \times 10^{-3} \exp(-0.48 \text{ eV kT}^{-1}) \text{ cm}^2 \text{ s}^{-1}. \quad (4)$$

At intermediate temperatures ranging from 702 to 1073 K, many controversial results on hydrogen diffusivity were reported with the maximum difference about five orders of magnitude at a fixed temperature. This difference is mainly due to the fact that the hydrogen diffusivity, at this temperature range, can be significantly influenced by the internal electric field, the interaction with dopants and other defects and etc [46]. A comprehensive discussion of discrepancies on hydrogen diffusivity data in this temperature range is given in the [43]. Furthermore, Hallam *et al* [43] also summarized the hydrogen diffusivity data from the literature, which is shown in figure 5. It is worth noting that at this temperature range, the hydrogen diffusivity is dominated by the diffusivity of interstitial hydrogen, as other forms of hydrogen diffuse very slowly as compared to the interstitial hydrogen.

At low temperatures ranging from 300 to 473 K, hydrogen transport in silicon is not dominated by atomic hydrogen, but by a mix of the diffusion of hydrogen dimers and the diffusion of excess hydrogen atoms, as reported by Saad *et al* [47]. It is found that hydrogen transport at these temperatures consisted of a fast diffusion specie, which is considered as excess interstitial hydrogen atoms in different charge states, and a slow diffusion specie, which is considered as excess hydrogen dimers or excess hydrogen-point defect complexes.

Interestingly, Kamiura *et al* [48] even reported hydrogen diffusivity at the temperatures below room temperature between 220 and 270 K, as expressed in equation (5). The authors attributed this diffusivity to the diffusivity of H^+ or H^0 and believed that H^0 has an activation energy of $\sim 0.5\ \text{eV}$ over a wide range of temperatures from 220 to 1473 K:

$$D_H = 7 \times 10^{-2} \exp(-0.54 \text{ eV kT}^{-1}) \text{ cm}^2 \text{ s}^{-1}. \quad (5)$$

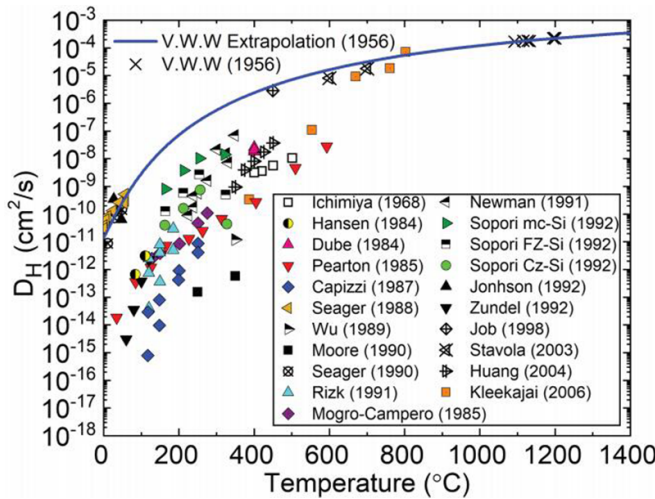


Figure 5. Hydrogen diffusivity data taken from the literatures. The solid line represents the extrapolation of the hydrogen diffusivity from the work of Wieringen *et al*. Reproduced from [37].

CC BY 4.0.

Importantly, it should be mentioned that hydrogen charge state plays an important role on interstitial hydrogen diffusivity. Theoretically, due to the coulomb attraction, the majority charge state of interstitial hydrogen will be attracted by ionized dopants at the moderate temperature range, leading to a lower diffusivity value. As evidences, Johnson *et al* [49] reported an activation energy of \$\sim 0.5 \text{ eV}\$ for \$\text{H}^+\$ and \$\sim 1.1 \text{ eV}\$ for \$\text{H}^-\$. In n-type (phosphorus doped) silicon sample, which has a good agreement with the reported activation energies for hydrogen diffusion without trap limiting effect and with that, respectively. It also easily implies that \$\text{H}^0\$ should have a better diffusivity as it is not affected by electric field. In experiment, Kamiura *et al* [30] reported an enhanced diffusivity of \$\text{H}^0\$ over \$\text{H}^+\$ and \$\text{H}^-\$ at 423 K about five orders of magnitude larger. More information regarding to the activation energies of various hydrogen charge state is well presented in [43].

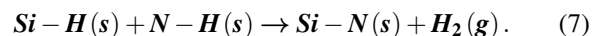
In summary, hydrogen diffusivity depends on many factors, including temperature, the form of hydrogen, charge states of interstitial hydrogen, electric field, the interaction with dopants and etc. At high temperatures above 1073 K, hydrogen diffusivity is determined by the diffusivity of interstitial hydrogen without any trap. At intermediate temperatures ranging from 702 to 1073 K, hydrogen still diffuses in the form of interstitial hydrogen, but its diffusivity is dramatically reduced by the interactions with dopants and defects. At low temperatures ranging from 300 to 473 K, hydrogen transport is dominantly in the form of hydrogen dimers and its diffusivity is very slow. In addition, hydrogen charge states play an important role on interstitial hydrogen diffusivity. It is reported that \$\text{H}^0\$ can diffuse faster than \$\text{H}^-\$ and \$\text{H}^+\$ about five orders of magnitude at 423 K.

2.5. Hydrogen source

Although hydrogen can be introduced into crystalline silicon by hydrogen plasma [50], hydrogen ion implantation [51],

forming gas annealing [52], firing the hydrogenated silicon nitride (\$\text{SiN}_x:\text{H}\$) [41], and chemical cleaning/etching [53, 54]. Noted that, firing the \$\text{SiN}_x:\text{H}\$ film to release hydrogen into crystalline silicon is widely used as the hydrogen source in photovoltaic industry. The reasons are three folds: (1) the \$\text{SiN}_x:\text{H}\$ film is a suitable anti-reflection coating due to the combination of good optical transparency and the tunable reflective index of the film; (2) the \$\text{SiN}_x:\text{H}\$ film is an excellent surface passivation layer and (3) the \$\text{SiN}_x:\text{H}\$ film can easily achieve silicon bulk passivation during the firing process. Other hydrogen sources have some disadvantages for their application in commercial solar cells. For example, hydrogen plasma and hydrogen ion implantation can introduce hydrogen atoms into crystalline silicon at a relative low temperature, but they can cause crystalline damage due to the high energy of the bombardment of hydrogen atoms from the equipment [55, 56]. Forming gas annealing will not cause crystalline damages, but it must be conducted at a relative high temperature exceeding 900 \$\text{°C}\$ [57]. Chemical cleaning/etching is conducted at a low temperature below 100 \$\text{°C}\$ and will not cause crystalline damage, but it can only introduce hydrogen into the surface of crystalline silicon roughly within 3 \$\mu\text{m}\$ of silicon surface [58]. In this paper, we mainly introduce the \$\text{SiN}_x:\text{H}\$ film as the hydrogen source due to its wide applications in industry.

The hydrogen within the \$\text{SiN}_x:\text{H}\$ film is dominantly bonded to the silicon atom or the nitride atom via the Si–H bond or the N–H bond. To detect them, it can typically use FTIR with the vibration frequency of the Si–H bond at \$\sim 2000\$–\$2250 \text{ cm}^{-1}\$ and the N–H bond at roughly \$3340 \text{ cm}^{-1}\$ and \$\sim 3450 \text{ cm}^{-1}\$ [59]. The release of hydrogen from the film is associated with a reconstruction of the film by the following reactions in equations (6) and (7):



When the hydrogen is released, the Si atom will form a bond with the N atom, resulting in the densification of the \$\text{SiN}_x:\text{H}\$ film. This is reflected in the FTIR absorption spectra with an enhancement in the Si–N peak (\$\sim 700\$–\$1020 \text{ cm}^{-1}\$, and with a reduction in the Si–H and N–H peaks at roughly 2250 and \$3300 \text{ cm}^{-1}\$, respectively) [60].

It is important to distinguish the silicon rich \$\text{SiN}_x:\text{H}\$ film and the nitride rich \$\text{SiN}_x:\text{H}\$ film, as they have distinct properties regarding to hydrogen. It was found that the silicon rich \$\text{SiN}_x:\text{H}\$ film contains more hydrogen in the as-deposited condition, however, after firing most of hydrogen escapes out of the \$\text{SiN}_x:\text{H}\$ film as hydrogen molecules due to the less dense film [61]. The nitride rich \$\text{SiN}_x:\text{H}\$ film contains less hydrogen, but most of hydrogen can diffuse into crystalline silicon in its atomic form due to the denser film [61]. Typically as reported in the literature [62, 63], the silicon sample coated with the silicon rich \$\text{SiN}_x:\text{H}\$ film has a better minority carrier lifetime in the as-deposited condition, whereas Si/N equal \$\text{SiN}_x:\text{H}\$ film can achieve the highest lifetime enhancement after firing. As an example, Chen *et al* [64] demonstrated the hydrogen content and the implied open circuit voltage (\$iV_{oc}\$) of the silicon

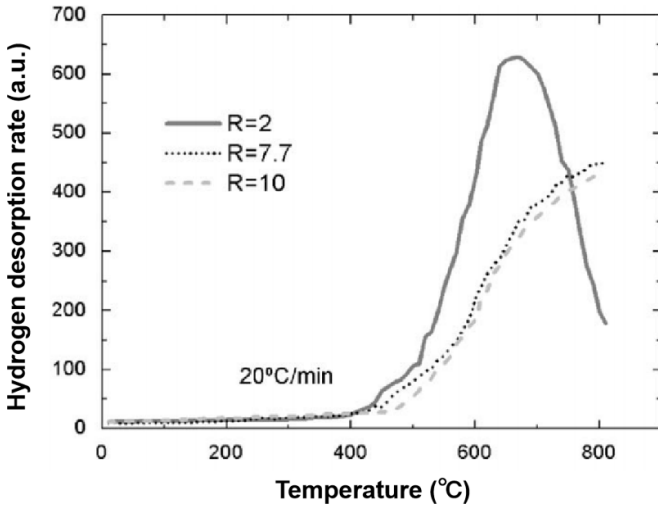


Figure 6. Hydrogen desorption rate as a function of the temperature characterized by temperature programmed desorption (TPD) for three different $\text{SiN}_x:\text{H}$ coatings (ammonia-to-silane gas flow ratio $R = \text{NH}_3/\text{SiH}_4$). Reprinted from [66], Copyright (2018), with permission from Elsevier.

sample coated with the different $\text{SiN}_x:\text{H}$ films at as-deposited condition and after firing. In detail, it was believed that the extent of bulk passivation is not related to the content of hydrogen within the $\text{SiN}_x:\text{H}$ film, but is instead associated with the in-diffusion of the atomic hydrogen to silicon bulk [65, 66]. It was found, experimentally, that high atomic density and high thermal stability of the $\text{SiN}_x:\text{H}$ film are key factors in determining the degree of bulk passivation achieved [59, 64]. Furthermore, the high thermal stability of the $\text{SiN}_x:\text{H}$ film is also significant to achieve high quality surface passivation as reported in [66]. In addition, the silicon rich and nitride rich $\text{SiN}_x:\text{H}$ films respond quite differently to the different firing temperatures in terms of the hydrogen desorption rate as shown in figure 6. It can conclude from figure 6 that the silicon rich $\text{SiN}_x:\text{H}$ film is able to release hydrogen at the relative low temperatures.

Firing temperature, during which hydrogen is released from the $\text{SiN}_x:\text{H}$ film, also plays a significant role on bulk passivation. For example, Yelundur *et al* [67] reported that different firing temperatures resulted in different lifetime enhancement factor for p-type string ribbon silicon, with the best performance enhancement occurring at the firing temperature of around 750 °C. Besides, Hameiri *et al* [68] investigated the effects of different firing temperatures on boosting the lifetime of Czochralsik silicon (Cz-Si) (non-specified wafer type in that paper) and found a similar trend with Yelundur *et al*. The reason is possibly that the firing temperature of around 750 °C can result in a maximum fractional concentration of H^0 in crystalline silicon during firing. In addition, the cooling rate of the firing process is critical to the performance of hydrogenation. For instance, Song *et al* [69] demonstrated that fast cooling rate and cooling with illumination can both promote the bulk hydrogenation performance.

In summary, the hydrogenated silicon nitride film ($\text{SiN}_x:\text{H}$) is the typical hydrogen source for crystalline silicon solar cells. The refractive index of $\text{SiN}_x:\text{H}$ film can be modulated to vary

the hydrogen content in $\text{SiN}_x:\text{H}$ film. Typically, the refractive index equal to 2 would be chosen for optimal anti-reflection property and good bulk passivation. Firing temperature also plays an important role on hydrogenation of silicon bulk with the best value at about 750 °C.

3. Applications of hydrogenation on deactivating/inducing defects

In section 2, the dominant properties of hydrogen in crystalline silicon are reviewed. In this section, we will expand the knowledge of hydrogenation on the mechanisms of how hydrogen passivates various kinds of defects for promoting the efficiency of silicon solar cells.

3.1. Dopant deactivation

Hydrogen is widely reported to be able to deactivate dopants. This can be advantageous if dopant density is too high to fabricate silicon solar cells with a reasonable efficiency. Experiments have found that the hydrogenation of dopant atoms will lead to a reduction in the free carrier concentration, but an increase in Hall mobility [70]. A model of hydrogenation of shallow dopants suggested that for boron–hydrogen pairs, the atomic hydrogen has bond center site geometry; and for phosphorus–hydrogen pairs, the atomic hydrogen has anti-bonding site geometry, due to the fact that the system needs to maintain the lowest energy geometry [70].

The schematic diagrams showing the bond structures of the H–B and H–P pairs are illustrated in figures 7 and 8.

In more detail, Chang *et al* [20] calculated H-dopant formation and dissociation energies as illustrated in figure 9, from which it is found that the dissociation energies are estimated to be roughly 0.1 eV and 0.6 eV for the H–P and H–B complexes, respectively. This result indicates that atomic hydrogen binds tighter with the boron atoms than the phosphorus atoms, and therefore it is relatively difficult to achieve a large fraction of phosphorus–hydrogen pairs in n-type silicon material.

It is worth noting that hydrogen-dopant complex is not stable at high temperature. In experiment, it was reported that at a temperature of around 473 K, reactivation of boron atoms will happen [71]. In addition, it is found [71] that carrier injection can accelerate the reactivation of boron atoms by converting H^+ to H^0 and then H^0 diffuses away from the boron atoms. The reports on the H–P complex are less, but the basic mechanism should be the same with the H–B complex.

Gallium-hydrogen (Ga–H) complex should exist in crystalline silicon, however, few reports studied the Ga–H complex in crystalline silicon. As far as the authors know, Lin *et al* [37] reported that Ga–H complex can act as the hydrogen source for the subsequent LeTID degradation in gallium doped PERC solar cells. Moreover, Kwapil *et al* [72] found that the different LeTID kinetics in gallium doped silicon was due to the different property of Ga–H complex.

In summary, hydrogen is able to deactivate dopants in crystalline silicon like boron and phosphorus. However, dopant–H

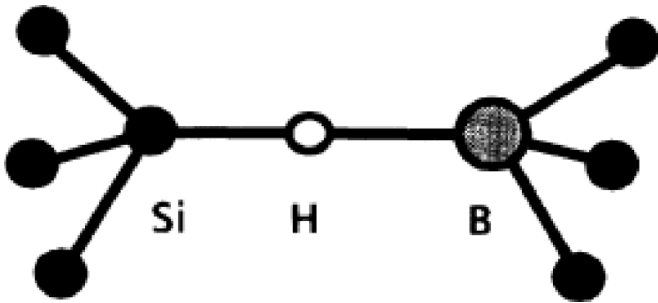


Figure 7. The schematic diagram showing the bond center geometry of the atomic hydrogen in a boron–hydrogen pair. Reprinted (figure) with permission from [71], Copyright (1988) by the American Physical Society.

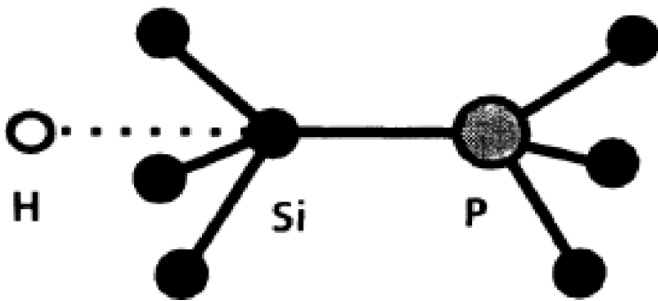


Figure 8. The schematic diagram of the anti-bonding site geometry of the atomic hydrogen in a phosphorus–hydrogen pair. Reprinted (figure) with permission from [71], Copyright (1988) by the American Physical Society.

complex is not stable, it can dissociate at elevated temperatures and under carrier injection.

3.2. Passivation of metallic impurity

Metallic impurities are common recombination centers in crystalline silicon, which are able to significantly reduce the efficiency of solar cells [73, 74]. Hydrogen is able to passivate most of metallic impurities in crystalline silicon and therefore attracted intense interest from researchers. Generally, hydrogenation of metallic impurity can eliminate the defect energy level induced by the metallic impurity or make it a shallow energy level.

One typical metallic impurity in crystalline silicon that can be hydrogenated is iron. For instance, Liu *et al* [17] reported that the concentrations of dissolved interstitial iron in p-type mc-Si wafers which covered with $\text{SiN}_x\text{:H}$ films were reduced by more than 90% after a 30 min anneal at the temperatures between 600 °C and 900 °C due to the formation of Fe–H complex, with the most effective reduction occurring at 700 °C, at which 99% of the initial dissolved iron is hydrogenated after 30 min. The mechanism is proposed to be the pairing of positively charged iron with negatively charged hydrogen, forming less recombination active Fe–H complexes in silicon. Later, Liu *et al* [75] also argued that some iron impurities might be gettered by silicon nitride film at that temperature range. Furthermore, Leonard *et al* [76] directly observed a DLTS

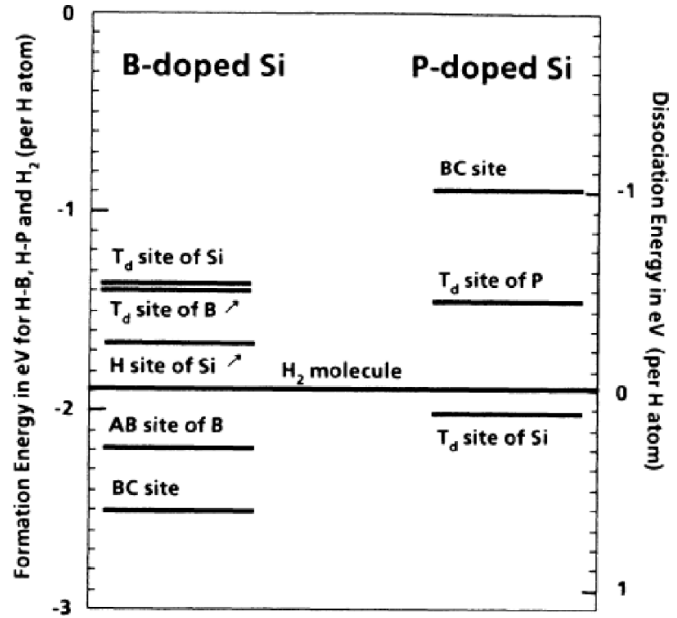


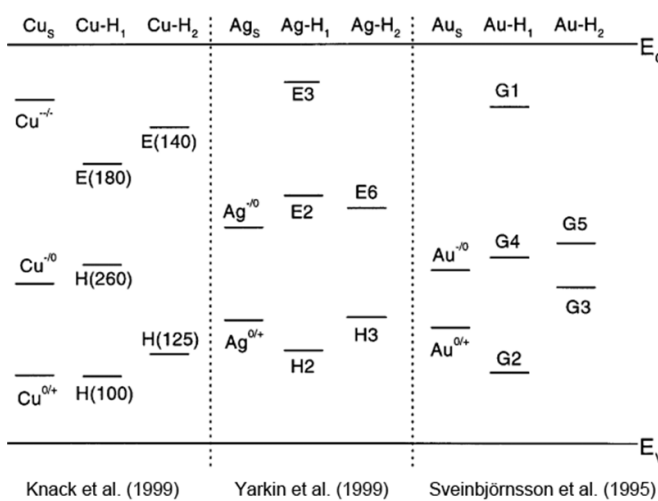
Figure 9. Calculated formation energies (left axis) and dissociation energies (right axis) for the H–B and H–P complexes and hydrogen molecules. BC (bond-center), T_d (interstitial tetrahedral), AB (anti bond-center). Reprinted (figure) with permission from [71], Copyright (1988) by the American Physical Society.

signal of Fe–H complex, which has a donor energy level at $E_v + 0.31$ eV. The DLTS results also indicated that the Fe–H complex has a temperature independent capture cross section at $5.2 \times 10^{-17} \text{ cm}^2$. This relative small capture cross section of Fe–H complex suggests that Fe–H complex has less recombination activity as compared to interstitial iron. It is worth noting that the Fe–H complex is extremely unstable and will dissociate completely by annealing for 30 min at 125 °C [77].

Hydrogenation of Cu, Ag, Au and Pt in crystalline silicon is as well vital since these four metallic impurities are ready to induce significant recombination in silicon. In the literature, Knack *et al* [78] used the DLTS to find the energy levels of the Cu–H complex. Two deep levels at $E_c - 0.36$ eV and $E_v + 0.54$ eV were attributed to the Cu–H₁ complex and a third charge state of this defect might be overlapping with the Cu donor energy level at $E_v + 0.21$ eV. For the complex of Cu–H₂, two energy levels at $E_c - 0.25$ eV and $E_v + 0.27$ eV were assigned. The authors also claimed that a passive hydrogen–copper complex can be formed, which contains three or more hydrogen atoms. Moreover, Einar *et al* [65] investigated the energy levels of Au–H complex via DLTS and found that Au and hydrogen can form two separate complexes, namely Au–H₁ complex and Au–H₂ complex. The Au–H₁ complex is electrically active and has three deep levels at $E_c - 0.19$ eV, $E_v + 0.21$ eV and $E_v + 0.47$ eV, respectively. In contrast, the Au–H₂ complex is electrically inactive. In addition, the authors found that the Au–H₂ complex dominated in the hydrogen rich region, whereas the Au–H₁ complex was present in hydrogen lean region. Furthermore, Yarykin *et al* [66] studied the Ag–H complexes in crystalline silicon by DLTS. In detail, the Ag–H₁ complex introduces

Table 1. The energy levels of the complexes of Cu, Ag, Au with hydrogen in crystalline silicon.

Species	Energy level 1	Energy level 2	Energy level 3
Cu-H ₁	$E_c - 0.36$ eV	$E_v + 0.54$ eV	$E_v + 0.21$ eV
Cu-H ₂	$E_c - 0.25$ eV	$E_v + 0.27$ eV	—
Cu-H ₃ or 4		Passive	
Ag-H ₁	$E_c - 0.45$ eV	$E_c - 0.09$ eV	$E_v + 0.28$ eV
Ag-H ₂	$E_c - 0.5$ eV	$E_v + 0.38$ eV	—
Ag-H ₃ or 4		Passive	
Au-H ₁	$E_c - 0.19$ eV	$E_v + 0.21$ eV	$E_v + 0.47$ eV
Au-H ₂		Passive	

**Figure 10.** The energy levels of copper, silver and gold and their complexes with hydrogen. Reprinted from [79], Copyright (1999), with permission from Elsevier.

three energy levels in the bandgap, which are $E_c - 0.45$ eV, $E_c - 0.09$ eV and $E_v + 0.28$ eV, respectively. The Ag-H₂ complex processes two energy levels at $E_c - 0.5$ eV and $E_v + 0.38$ eV, respectively. The electrically inactive Ag-H complex includes at least three hydrogen atoms and can be annealed out at roughly 450 °C. Overall, the energy levels of Cu, Ag, Au and their complexes with hydrogen are listed in table 1 and illustrated in figure 10. At last, Sachse *et al* [79] reported four platinum-hydrogen related deep levels identified at $E_c - 0.18$ eV, $E_c - 0.50$ eV, $E_v + 0.30$ eV and $E_v + 0.40$ eV by DLTS, respectively. These levels belong to at least three different platinum-hydrogen complexes and all of them are electrically active. Nevertheless, the exact number of hydrogen in the platinum-hydrogen complex for each energy level is not identified in that paper. Moreover, according to the above results, it can hypothesize that multiple H-metal impurity complex is more likely to be passive and the method to incorporate multiple hydrogen into the complex would be a hydrogen rich environment for the reaction.

Some other metallic impurities can interact with hydrogen as well in crystalline silicon, although they might play a less important role on the electrical quality of silicon wafer.

To make the paper brief, the energy levels of these metallic impurities and their complexes with hydrogen are summarized in figure 11 [80].

It is worth noting that metallic impurities and hydrogen can exhibit different charge states and electrical properties in n- and p-type crystalline silicon and even with different dopants such as with Ga. Typically the interstitial hydrogen with a different charge state to metallic impurities can deactivate them better [80]. Furthermore, different dopants might change the activation energy required for the hydrogenation of the metallic impurities.

In summary, hydrogen is able to passivate diverse metallic impurities in crystalline silicon. Typically, hydrogen-metal impurity complex is still recombination active with one hydrogen in the complex, but with more hydrogen attaching to the metallic impurity the complex becomes recombination inactive with no defect energy level in silicon bandgap.

3.3. Passivation of extended defects

Extended defects are detrimental to silicon solar cells, as they are able to reduce minority carrier lifetime and induce shunt paths across the p-n junction [81, 82]. In the worst case, metallic impurities can segregate into the extended defects to enhance their recombination activity [83]. In experiment, Sopori *et al* [84] demonstrated that dislocation clusters in back surface field silicon solar cells can lead to an efficiency loss of more than 3–4 absolute percentage points.

Hydrogen is able to effectively passivate extended defects in multi- and cast-mono crystalline silicon wafers [85]. In previous reports, Dube and Hanoka [81] reported that hydrogen was able to passivate dislocations for depths up to 250 μm in string ribbon silicon. Furthermore, Weronek *et al* [86] reported the hydrogenation of the extended defects-related D-Band luminescence in silicon. In detail, it was found that hydrogenation at 300 °C are able to reduce the D1 and D4 band intensities but increase the intensities of the D2 and D3 bands. In the paper, the D1 and D2 bands are assigned to a recombination at the stacking fault between relaxed partials and the D4 band is assigned to the zero-phonon transition of a localized state at the dislocation and the D3 band is assigned to the momentum conserving TO-phonon replica of the D4 band. Furthermore, it is reported that hydrogenation of extended defects can be enhanced by an additional illuminated annealing process. For instance, Song *et al* [80] demonstrated that a post-firing annealing at 350 °C and 9.6×10^{18} photons $\text{cm}^{-2} \text{ s}^{-1}$ illumination intensity for 4 min can dramatically enhance the passivation effectiveness of extended defects by hydrogen, of which the LBIC maps before and after the treatment are shown in figure 12. This result indicates that a short firing process is not sufficient to completely passivate extended defects.

Although hydrogen is able to passivate extended defects, the effectiveness of passivation depends on some key factors. The first key factor is whether the extended defects are decorated with metallic impurity or not. In the literature, Martinuzzi *et al* [21] found that there exists two types of defects associated

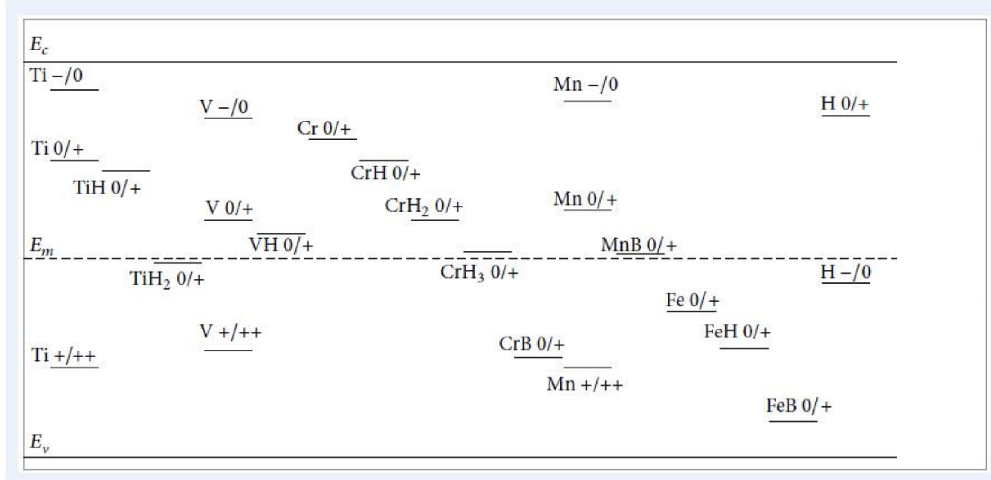


Figure 11. The energy levels of some metallic impurities and their complexes with hydrogen in silicon bandgap. Reproduced from [84]. CC BY 3.0.

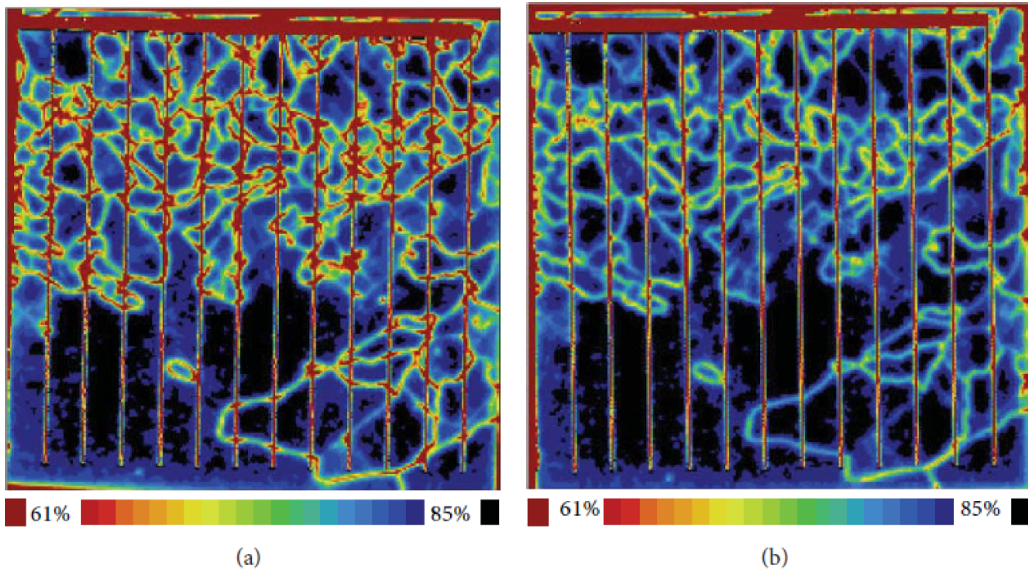


Figure 12. The 981 nm spatial internal quantum efficiency maps of the cell before (a) and after (b) the illuminated annealing process. Reproduced from [84]. CC BY 3.0.

with the extended defects in silicon, namely deep level defects and shallow level defects. It is reported that the shallow level defects could be completely passivated by hydrogen, whereas deep level defects were transformed into shallow one after hydrogenation. We hypothesize that the shallow level defects might be associated with the part of extended defects without metallic impurity decoration, whereas the deep level defects might be associated with the part of extended defects with metallic impurity decoration. The experimental observations of deep and shallow level defects are shown in figure 13. It is evident that deep level defects appear in room temperature (300 K) LBIC scan map, whereas shallow level defects appear in low temperature (100 K) LBIC scan map. Furthermore, figure 14 reveals the different response of hydrogenation on deep level defects and shallow level defects. Please note that the LBIC contrast (C) is defined according to equation (8),

based on the electron-beam induced current scan maps by the ratio:

$$C = 1 - I_{\text{def}}/I_0. \quad (8)$$

where I_{def} is the current collected at a defect and I_0 is the background current. By the comparison of figures 14(a) with (b), it shows that some part of extended defects are well passivated by hydrogen and this part is assigned to shallow level defects, whereas other part of extended defects cannot be passivated by hydrogen and are assigned to deep level defects. To get more insight on the influence of metallic impurity on hydrogenation of extended defects, we review the reports from Kittler *et al* [87]. It is found that metallic impurities accommodated in the extended defects core cannot be hydrogenated, whereas the metallic impurities in the cloud surrounding the extended

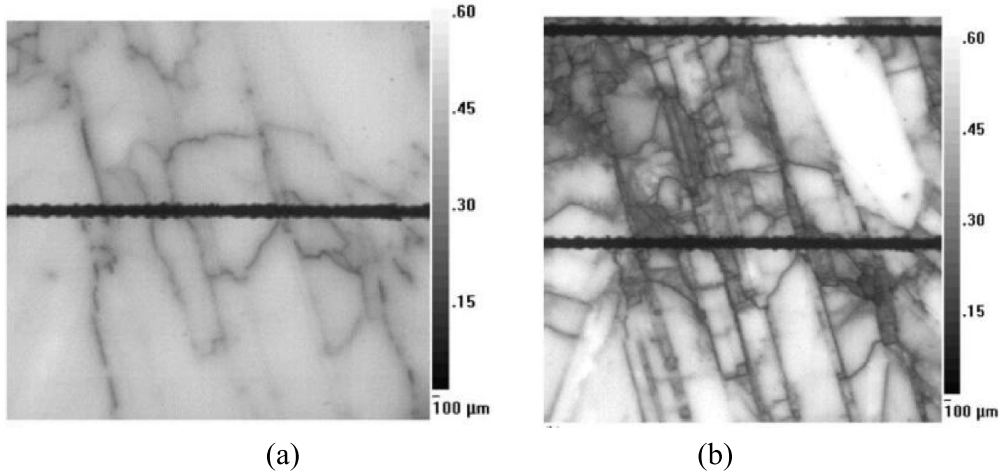


Figure 13. LBIC scan maps at (a) 300 K and (b) 100 K of a part of the $\text{SiN}_x:\text{H}$ cell in figure 14, which indicates that two kinds of defects, namely shallow level defects and deep level defects, exist in crystalline silicon. Reprinted from [21], Copyright (2003), with permission from Elsevier.

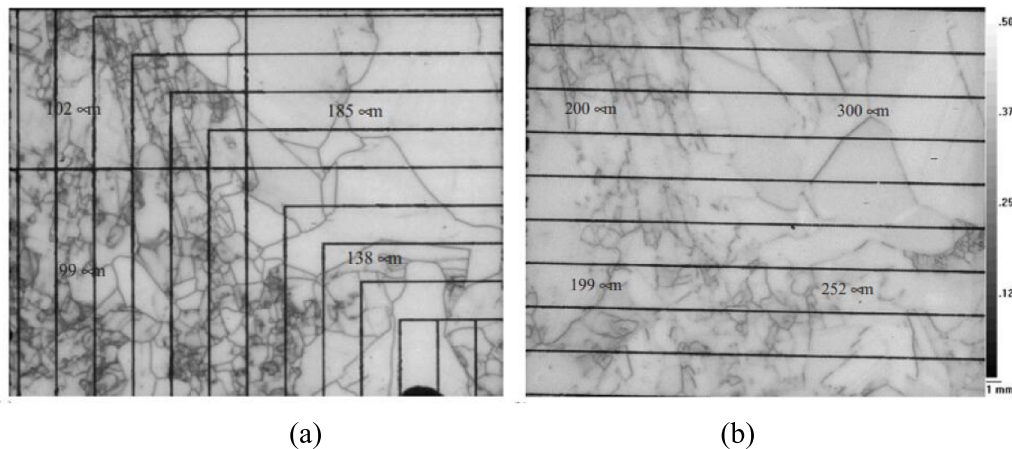


Figure 14. (a) LBIC scan map of a TiO coated cell at room temperature. The LBIC contrast at GBs and dislocation lineages or tangles is marked. This TiO coated cell corresponds to the cell without hydrogenation. (b) LBIC scan map of a $\text{SiN}_x:\text{H}$ coated cell (made up of sister wafers with figure (a) at room temperature). The contrast at defects is neatly attenuated by hydrogenation. Reprinted from [21], Copyright (2003), with permission from Elsevier.

defects are weakly bound and can be passivated by hydrogen. In our opinion, we interpret this result as that the metallic silicide are strongly bound and cannot be passivated by hydrogen, whereas the metallic precipitates around the extended defects can be passivated by hydrogen.

In addition, the second key factor is the hydrogenation conditions. For instance, Rinio *et al* [88] compared the effectiveness of hydrogenation of extended defects via the methods of either firing the $\text{SiN}_x:\text{H}$ layer or applying a microwave induced remote hydrogen plasma (MIRHP). As a conclusion, firing the $\text{SiN}_x:\text{H}$ layer has better hydrogenation performance than MIRHP, but the best performance was achieved by the combination of these two methods. It can conjecture from this result that some defects in extended defects require high temperature to trigger hydrogenation, which corresponds to a high activation energy of this reaction, whereas other defects in extended defects require a relative long time to deactivate it due to the low reaction rate. Therefore it is crucial

to carefully manipulate temperature and time to effectively passivate extended defects by hydrogen. In addition, Ciesla *et al* [22] found that the illuminated annealing, which boosts the fractional concentrations of H^0 and H^- , can dramatically enhance the performance of hydrogenation on extended defects in p-type cast mono-like silicon, as compared to dark annealing.

In summary, hydrogen is able to passivate extended defects in crystalline silicon, but its effectiveness depends on two key factors: the contamination level and the hydrogenation conditions. Therefore, careful manipulation of hydrogenation conditions and pre-gettering step are vital for maximizing the performance of hydrogenation on extended defects.

3.4. Passivation of grain boundary

GB is another dominant lifetime-limiting defect in multi- and cast-mono crystalline silicon. In general theory, GB can be

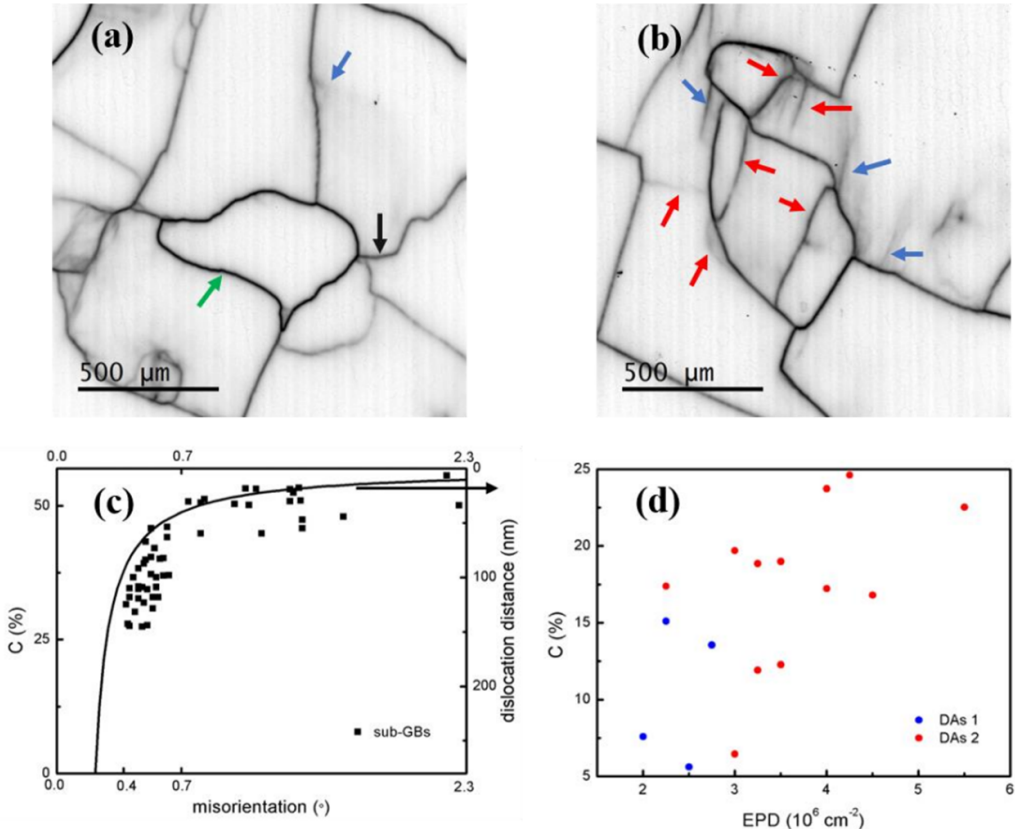


Figure 15. (a), (b) EBIC images of two as-grown CM–Si samples at 300 K. The green arrow is sub-GB (mis-orientation $>0.7^\circ$), the black arrow is also sub-GB, but mis-orientation $<0.7^\circ$. The blue arrows are DAs (dislocation arrays) 1, and the red arrows are DAs 2. (c) The changes in dislocation distance and EBIC contrast (C) at 300 K of sub-GBs with respect to the mis-orientation in the as-grown CM–Si. (d) Variation of EBIC contrast (300 K) of DAs with etch pits density (EPD) in the as-grown CM–Si. Reproduced from [94]. © IOP Publishing Ltd. All rights reserved.

classified into two categories: small angle (SA) GB with mis-orientation angle $<15^\circ$ and large angle (LA) GB with mis-orientation angle $\geq 15^\circ$.

For more details of SA GB, Mao *et al* [89] provided some information about its recombination activity. They investigated the recombination activities of SA GB in cast mono silicon (CM–Si) and found that the recombination activity of SA GB increased with the mis-orientation angle and saturated at the mis-orientation angle above 0.7° , as shown in figure 15. The reason is hypothesized that the dislocation density associated with the SA GB increased with the mis-orientation angle and so did the dangling bonds inside the SA GB until 0.7° .

For LA GB, the recombination activity of LA GB is weak when it is in low contamination level. Nevertheless, when the LA GB is contaminated with metallic impurity heavily, LA GB shows a strong recombination activity. Nevertheless, it is worth noting that typically LA GB has a strong ability to getter metallic impurities into it and therefore induce strong recombination activity.

Hydrogenation is an effective way to passivate GB, but the passivation mechanisms vary dramatically to different defects in GB. In the literature, it is reported that both impurity contamination level and the GB character can strongly influence the hydrogenation mechanisms on GB. To get insight into the mechanism, the authors reviewed lots of reports in the

literature and concluded three assumptions for the hydrogenation of GB.

- (a) Dangling bonds in GB can be well passivated by hydrogen by removing its defect energy level out of silicon bandgap.
- (b) Metallic silicide inside GB cannot be passivated by hydrogen.
- (c) Metallic precipitates in the GB core can be passivated by hydrogen in terms of transforming its defect energy level from deep to shallow.

To find the evidences to support these three assumptions, we conclude the following reports from the literature.

- (a) Dangling bonds in GB can be well passivated by hydrogen by removing its defect energy level out of silicon bandgap

Johnson *et al* [38] provided the direct evidence to support the fact that hydrogen is able to passivate the dangling bonds in GB via using the characterization tool of electron-spin resonance. After hydrogenation, it is found that the passivated dangling bonds in GB are no longer active. In addition, Chen *et al* [90] found the evidence that hydrogen can completely passivate the dangling bonds in GB. They demonstrated that

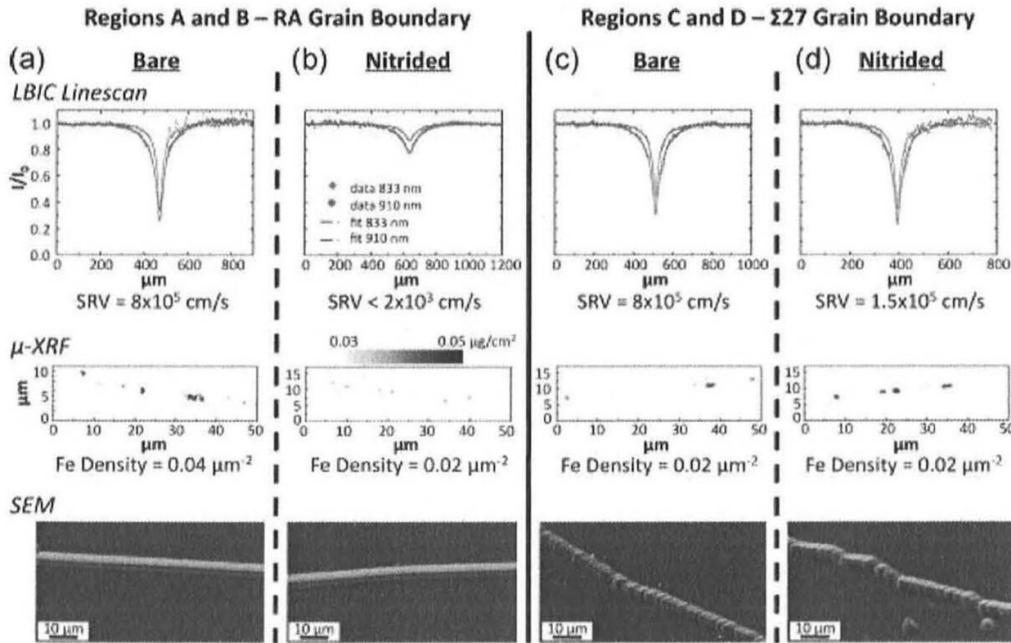


Figure 16. Comparison of passivated and non-passivated grain boundaries before and after hydrogenation, SRV (surface recombination velocity). [97] John Wiley & Sons. © 2015 WILEY-VCH Verlag GmbH & Co. KGaA, Weinheim.

the multi-crystalline silicon (mc-Si) wafers with low Fe contamination can be well passivated by hydrogen, leading to that the EBIC contrast decreased about 75%–80% for the Σ ($\Sigma = 3, 9$, and 27) GBs and decreased about 35%–40% for the small angle (SA) and random angle (RA) GBs. As the impurity contamination level is low, it is reasonable to assume that the 75%–80% reduction of EBIC contrast in the Σ ($\Sigma = 3, 9$, and 27) GBs is due to the hydrogenation of clean dangling bonds. Other researchers reported some evidences as well. For instance, Park *et al* [24] reported that hydrogenation can reduce the density of dangling bonds in clean GB by about a sevenfold. In addition, Maydell *et al* [91] confirmed that hydrogen can terminate the dangling bonds in GB to dramatically reduce the GB recombination activity. Nevertheless, no DLTS result is available to reveal the elimination of the defect energy level of dangling bonds in GB by hydrogen.

(b) Metallic silicide inside GB cannot be passivated by hydrogen

Although GB can be passivated by hydrogen, the recombination activity of some parts in GB still exists after hydrogenation. Subjecting to this observation, the authors hypothesize that the metallic silicide in GB cannot be passivated by hydrogen. Some reports in the literature can support this assumption. For example, Chen *et al* [90] demonstrated that even after efficient hydrogenation, all types of GB exist some recombination activity, indicating some defects cannot be passivated by hydrogen. Moreover, Buonassisi *et al* [92] found that hydrogenation is particularly effective for random angle (RA) GB, but is with almost no passivation effect on low coincidence site lattice (CSL) GB, as shown in figure 16. The reason is explained by that the RA GB has less dangling bonds and

therefore less metallic silicide is formed inside it, whereas low CSL GB contains more dangling bonds and therefore more metallic silicide inside it. As the metallic silicide cannot be passivated by hydrogen, the hydrogenation performance on the low CSL GB would be low. Furthermore, Yu *et al* [93] found an interesting result that hydrogenation can reduce the density of GB states, but cannot significantly influence the distributions of its defect energy levels and the associated carrier capture cross-sections, which suggests that hydrogen can only passivate clean dangling bonds, but cannot deactivate the metallic silicide in the GB core.

(c) Metallic precipitates in the GB core can be passivated by hydrogen in terms of transforming its defect energy level from deep to shallow

Even in heavily contaminated samples, hydrogenation is able to reduce the density of GB states to some extent. The authors hypothesize that the metallic precipitates in the GB can be passivated by hydrogen and after passivation the associated defect energy level is transformed from deep to shallow. Some reports in the literature can support this assumption. For example, Jiang *et al* [25] investigated the impact of hydrogenation on the electrical properties of a GB (with metallic precipitates) in the p-type direct silicon bonded wafers by using current–voltage (*I*–*V*) and DLTS tools. It was found that the energy distributions of interfacial states in GB after hydrogenation became shallower, and the majority carrier capture cross-section was reduced by approximately two orders of magnitude, whereas the density of GB states varied only slightly. This phenomenon indicates that a certain defect in GB, most likely metallic precipitates, can be partially passivated by hydrogen by transforming its defect energy level from deep to

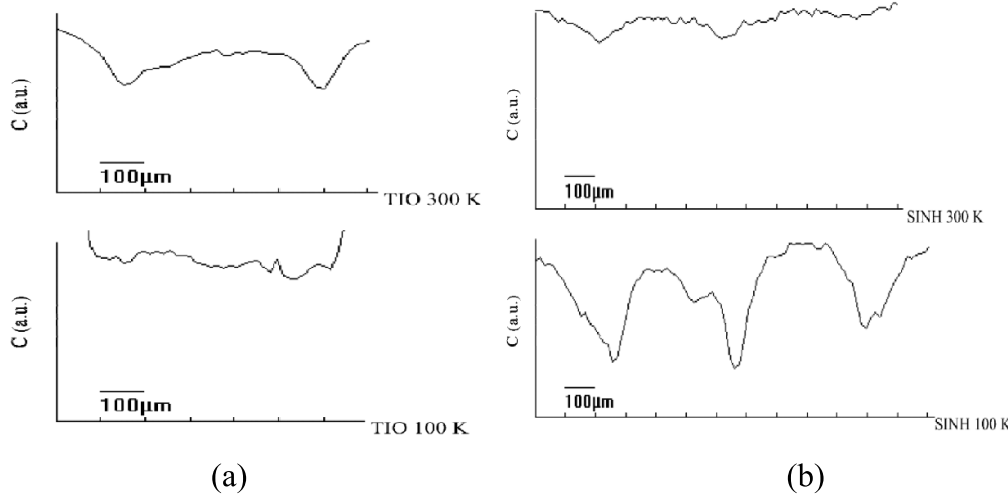


Figure 17. The EBIC contrast (C) of the sample at 300 K and 100 K (a) when the sample is coated with TiO antireflection coating (without hydrogenation) and (b) when the sample is coated with $\text{SiN}_x:\text{H}$ layer (with hydrogenation). Reprinted from [21], Copyright (2003), with permission from Elsevier.

shallow. In addition, Martinuzzi *et al* [94] demonstrated that hydrogenation indeed transformed the defect energy level of GB from deep to shallow, indicated by the EBIC contrast (C, defined by equation (8)) variations at 300 K and 100 K before and after hydrogenation as illustrated in figure 17. Please note in figure 17 that deep energy level defects dominated in 300 K EBIC scan before hydrogenation, whereas after hydrogenation the shallow energy level defects dominated in EBIC scan at 100 K.

In summary, GB can exhibit distinct recombination activity due to the different GB character and the contamination level. Hydrogen is able to effectively passivate GB, but the mechanism of hydrogenation on GB varies significantly for the different defects. To better understand hydrogenation of GB, three assumptions are made to explain the above mechanism. These three assumptions are: (a) dangling bonds can be completely passivated by hydrogen by removing its defect energy level out of silicon bandgap; (b) metallic silicide in GB cannot be passivated by hydrogen; (c) metallic precipitates in GB can be passivated by hydrogen in terms of transforming its defect energy level from deep to shallow.

3.5. Passivation of silicon surface states

Surface passivation is another important issue for crystalline silicon, as it can influence the efficiency of silicon solar cells to a large extent. Typically, the silicon surface states are well passivated by surface passivation layer or stack such as the hydrogenated silicon nitride film or the aluminum oxide film or the stack of them. Nevertheless, to obtain ultrahigh open circuit voltage of the cell, it is still necessary to further reduce the density of silicon surface states by hydrogenation even after the coating of passivation layer.

Hydrogen is able to passivate both the clean silicon surface states and the contaminated silicon surface states. For instance, Leguijt *et al* [94] reported that the density of interface states D_{it} , in the clean silicon surface, can be strongly

reduced by the hydrogenation step, and a low D_{it} value in the order of $10^{10} \text{ cm}^{-2} \text{ eV}^{-1}$ can be obtained after hydrogenation. In addition, Hezel *et al* reported that the hydrogenation step resulted in the lowest value of D_{it} of $8 \times 10^9 \text{ cm}^{-2} \text{ eV}^{-1}$ (at midgap), whereas as-deposited $\text{SiN}_x:\text{H}/\text{Si}$ interface showed D_{it} value between 10^{11} and $2 \times 10^{12} \text{ cm}^{-2} \text{ eV}^{-1}$. The above observations suggest that hydrogenation can further reduce the density of silicon surface states even after the coating of passivation layer. To find the mechanism of hydrogenation on silicon surface states, Chris *et al* [95] calculated the binding energies of various H configuration in silicon, and found that Si–H is a relative stable bond, as shown in figure 18. Furthermore, Cartier *et al* [96] demonstrated that atomic hydrogen can passivate silicon surface states, but at the meantime the Si–H bond dissociates. They further found that the dissociation of Si–H bond in silicon surface can be enhanced by carrier injection. For the contaminated silicon surface states, hydrogenation of them becomes a complex mechanism. In detail, Oura *et al* [97] demonstrated that the interaction of atomic hydrogen with the metal-silicon sub-monolayer interfaces results in the agglomeration of the two-dimensional metal layers into the three-dimensional metal islands, as shown in figure 19. It is worth noting that the phenomenon confirmed by Ag/Si system may not fit into all metals/silicon system. Nevertheless, the literature about other metals/silicon system is relatively few.

In summary, hydrogen is able to passivate silicon surface states both with and without contamination. For clean silicon surface, hydrogenation can reduce the density of silicon surface states to several folds smaller. For contaminated silicon surface, hydrogenation can result in the agglomeration of the two-dimensional metal layers into the three-dimensional metal islands.

3.6. Passivation of boron–oxygen related defects

Boron–oxygen related defects can dramatically reduce the efficiency of boron-doped, oxygen-rich Cz-Si solar cells and

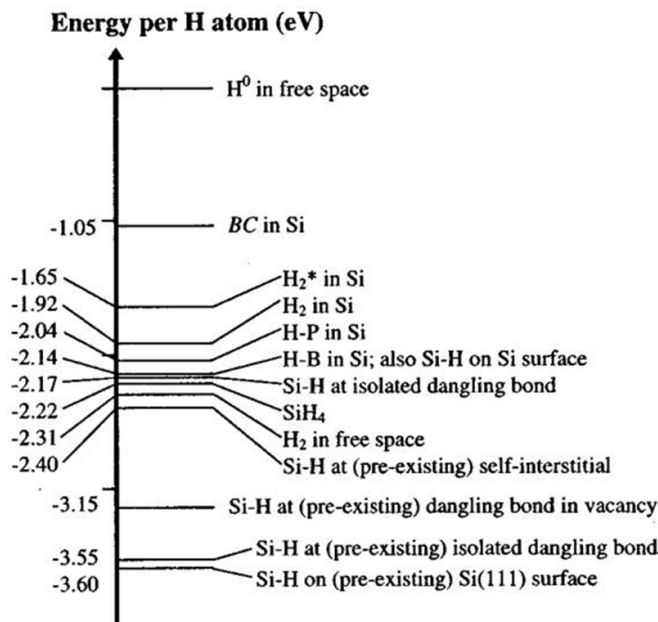


Figure 18. First-principles energies for various configurations of H in Si. The zero of energy corresponds to a free H atom. The energy values were determined with first-principles pseudopotential-density-functional calculations, and include zero-point energies. Please note that BC stands for bond-center and H_2^* means a metastable hydrogen dimer. Reprinted from [103], Copyright (2016), with permission from Elsevier.

therefore get intense interest from photovoltaic researchers. Up to date, researchers found that the B–O related defects are made up of substitutional boron and interstitial oxygen dimer. Light induced degradation (LID) that caused by B–O related defects consists of a fast degradation process and a slow degradation process and the degradation mechanism is identified as a configuration change of the B–O related defects. Since the characteristics of the B–O related defects are not the focus of this paper, we will only introduce the hydrogenation of B–O related defects in this section. More information about the characteristics of B–O related defects can be found elsewhere [98–101]. In addition, the B–O related defects can be deactivated by two ways. One way is the dissociation of the B–O related defects by dark annealing. Another way is to permanently passivate the B–O related defects via an illuminated annealing process, through which the B–O related defects are turned to a recombination inactive ‘regenerated’ state [100]. This regeneration process is the focus of this section and it requires hydrogen to participate in [100].

To better understand the regeneration process, we start with the introduction of three state model of B–O related defects. Herguth *et al* [102] first put forward the three state model for describing the long-term behavior of the metastable B–O related defects in crystalline silicon, as shown in figure 20.

From the three state model, it can be seen that state B is the degraded state and it can be transformed to state A (annealed state) by dark annealing. The transformation from state B to state A is also found experimentally at the conditions of elevated temperature and carrier injection, and is often called the

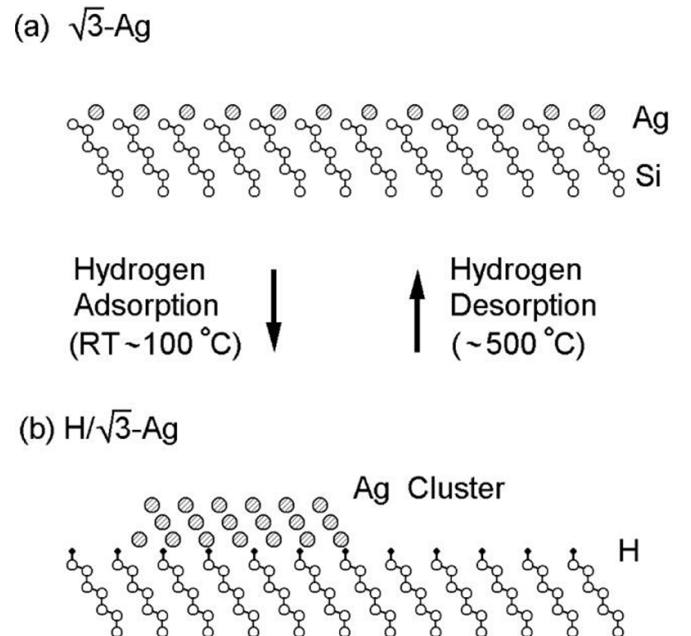


Figure 19. Schematic illustration of the side view of (a) Si(111) $\sqrt{3} \times \sqrt{3}$ -Ag surface and (b) hydrogen-induced Ag(111) crystallites grown epitaxially on the H-covered Si(111) substrate. Structural transformation between these two structures is reversible with the adsorption and desorption of atomic hydrogen. Reprinted from [101], with the permission of AIP Publishing.

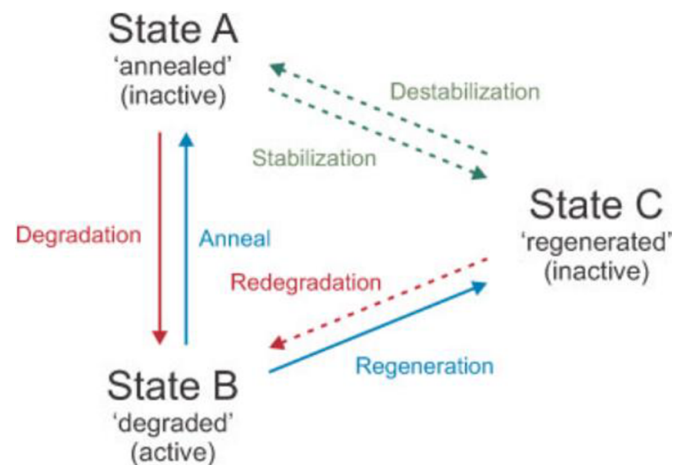


Figure 20. The three state model of the metastable B–O related defects in crystalline silicon. © 2006 IEEE. Reprinted, with permission, from [109].

regeneration process. The transformation from state A to state B is the typical LID process. The transformation from state C to state B is also possible and can occur at high temperature above 200 °C, and is called the redegradation process. Other transformations such from state A to state C and from state C to state A are considered as impossible by Hallam *et al* [103]. They studied the kinetics of the LID and regeneration processes of B–O related defects, and found strong evidences that no direct passivation pathway occurs for the passivation from state A to state C. In addition, the transformation from state C to state A can be well described by the kinetics of the

transformations from state C to state B and then from state B to state A, therefore they considered the transformation from state C to state A less likely.

Among all the transformations, the regeneration process from state B to state C is of great importance. As this transformation can permanently deactivate the B–O related defects, which means that LID will not occur under normal field operation. The mechanism of the regeneration process is extensively studied. Typically, two hypotheses are considered to cause the regeneration process, namely boron nano-precipitates induced regeneration and hydrogen induced regeneration. For the first hypothesis, Walter *et al* [104] suggested that boron nano-precipitate is a candidate for the regeneration process as it is known that plasma treatment can generate boron nano-precipitate in crystalline silicon and plasma treatment is confirmed to be necessary for the regeneration process. Nevertheless, recent work by Nampalli *et al* [28] suggested that hydrogen rather than boron nano-precipitate is more likely to be responsible for the regeneration process. The evidence is that the regeneration process cannot occur when the sample is subjected to the plasma treatment without hydrogen source, which can still generate boron nano-precipitate in silicon. Whereas the regeneration process does occur with hydrogen present in silicon bulk.

Regarding to the role of hydrogen on the regeneration of B–O related defects, more interesting works are reported. In detail, Wilking *et al* [29] studied the high-speed regeneration process and suggested that the boron–hydrogen pairs are the hydrogen source for the regeneration reaction. Another work by Wilking *et al* [29] found that uncharged H^0 is directly responsible for the permanent passivation of B–O related defects and therefore the regeneration rate is dependent on the concentration of uncharged H^0 rather than the total concentration of monatomic hydrogen in silicon. Recent studies also explored the possibility of rapid regeneration process for industrial applications, which is able to completely deactivate the B–O related defects within 10 s. For example, Wilking *et al* [29] found that temperature range of 200 °C and 230 °C at 2.7 suns can completely deactivate the B–O related defects in less than 3 s. Furthermore, Hallam *et al* found that laser can accelerate the formation of B–O related defects and subsequent permanent passivation of it, which reduced the total processing time from approximately 170 s to 10 s.

Other studies calculated the activation energy of the regeneration process. In detail, various studies presented a wide range of values for the activation energy of the regeneration process, such as 0.6 eV, 0.7 eV, 1.0 eV and 1.2 eV with all the studies claiming uncertainty ranges below 0.1 eV [105]. This phenomenon is consistent with the hypothesis by Herguth *et al* [106] that the regeneration process at low and high temperatures might be different and has different activation energies.

In summary, B–O related defects are typical LID defects in crystalline silicon. Passivation of B–O related defects is crucial as it can significantly enhance the stable efficiency of solar cells. There are two kinds of passivation for B–O related defects, namely unstable passivation of B–O related defects and permanent passivation of B–O related defects. Permanent passivation of B–O related defects gets more interest

from researchers as the degradation does not occur after permanent passivation. It is found that permanent passivation requires hydrogen to participate in and the detailed mechanism might be hydrogen bonding with B–O related defects to form a recombination inactive complex. Recent studies also suggested that H^0 is directly responsible for permanent passivation and therefore carrier injection can dramatically enhance the rate of permanent passivation.

3.7. Possible role of hydrogen in LeTID

Except for the typical LID induced by B–O related defects, recent studies found that crystalline silicon also suffers from LID in the conditions of light and elevated temperature, which is named LeTID. LeTID is sometimes referred to carrier induced degradation (CID) as it also occurs under current injection at elevated temperature. LeTID exhibits many specific behaviors, such as the dependence on peak firing temperature and cooling rate, the possibility to be modulated by dark annealing and etc. These interesting behaviors will be discussed later. Researchers also attempted to find out the mechanism of LeTID in crystalline silicon, however, up to date, the defects responsible for LeTID is still unknown. Nevertheless, researchers still put forward two hypotheses to explain the mechanism of LeTID. Among them, hydrogen is identified as an ensured candidate to participate in LeTID.

To confirm the participation of hydrogen in LeTID, at first, Bredemeier *et al* [107] compared the behaviors of LeTID in wafers fired at 900 °C and 650 °C, and only found the degradation in wafers fired at 900 °C. Chan *et al* [108] further reported that LeTID could be observed only when the peak firing temperature exceeded 700 °C. These phenomena indicate that a species released from the firing process can trigger LeTID, which is most likely hydrogen. Second, Schmidt *et al* [109] found a direct correlation between the extent of LeTID and the amount of hydrogen within silicon bulk (as shown in figure 21), which confirmed that hydrogen participated in LeTID. Third, Chan *et al* [110] found that post-firing dark annealing can alter the subsequent LeTID degradation and regeneration. In detail, dark annealing at the temperatures of 200 °C or below for 2.5 h was found to accelerate the degradation and regeneration rates and the degradation severity, whereas after dark annealing at higher temperatures (above 200 °C) a new defect with a substantially longer degradation and regeneration rates emerged. This behavior is consistent with the behavior of hydrogen in silicon. Fourth, Jensen *et al* [111] found that hydrogen must be present in the silicon bulk for the occurrence of LeTID in multicrystalline silicon (mc-Si), as shown in figure 22. Please note that ‘fired’ means the sample gets MIRHP treatments first and then gets fired to let hydrogen diffuses out of silicon bulk.

The detailed role that hydrogen plays in triggering LeTID is discussed in some recent works. In detail, Weiser *et al* [112] used infrared (IR) spectroscopy to detect the vibrational signatures due to the H–B, H–Ga, and $H_2^*(C)$ (a metastable hydrogen dimer) defects in p-type mc-silicon wafers, and found that LeTID degradation would reduce the concentrations of H–B, H–Ga (as shown in figure 23), and therefore inferred that the

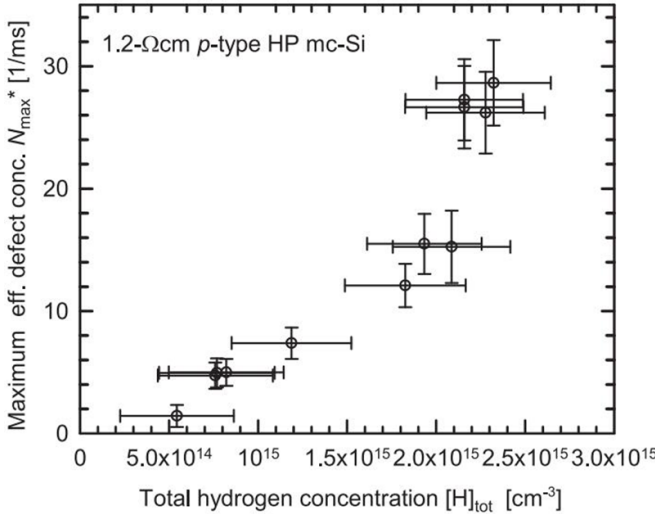


Figure 21. Maximum effective defect concentrations N_{\max} measured on neighboring HP mc-Si sister wafers, which were coated on both surfaces with $\text{SiN}_x:\text{H}$ films of different Si:N ratios and fired at 900°C . N_{\max} is plotted versus the total hydrogen content $[\text{H}]_{\text{tot}}$ measured on boron-doped FZ-Si wafers, which were processed in parallel to the mc-Si wafers. © 2019 IEEE. Reprinted, with permission, from [117].

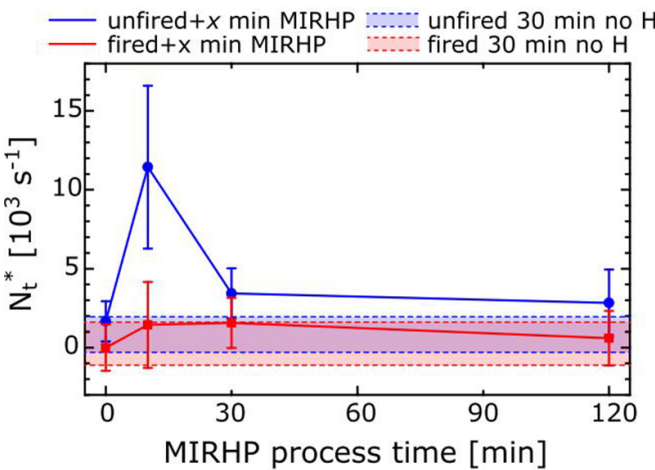


Figure 22. Maximum effective defect density (N_t^*) measured for the unfired and fired samples as a function of microwave-induced remote hydrogen plasma (MIRHP) process time in minutes. Longer MIRHP process time corresponds to higher hydrogen concentration. For samples where MIRHP time was not varied (unfired and fired 30 min MIRHP time with no H), the minimum and maximum N_t^* bounds are plotted as shaded areas. Reprinted from [119], with the permission of AIP Publishing.

hydrogen attended in LeTID might come from the H–B and H–Ga pairs. In addition, Chen *et al* [113] found a similarity in defect formation and recovery kinetics in both p-type and n-type silicon, and inferred that the behavior of LeTID both in the dark and under illumination might be explained by the interactions between charged hydrogen species and dopant atoms within the diffused layers and the silicon bulk. Furthermore, recent work by Lin *et al* [30] proposed a new model to explain LeTID. In their model, a simple reversible

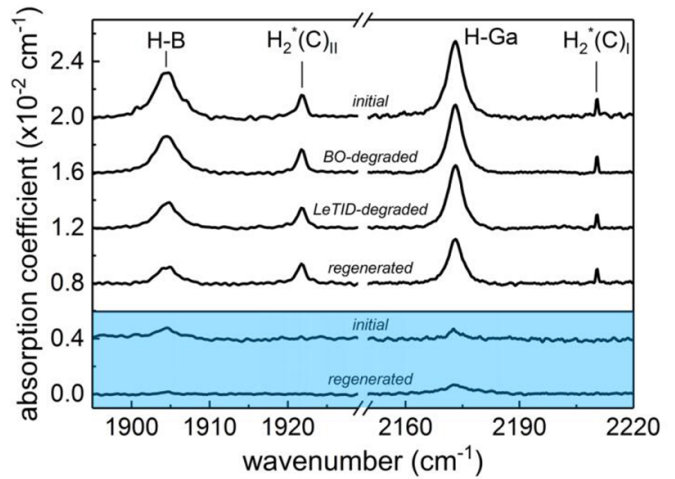


Figure 23. IR absorption coefficient spectra (5.0 K , $\text{res} = 0.5\text{ cm}^{-1}$) of high performance mc-Si samples (bottom panel = non-hydrogenated, top panel = hydrogenated) in different stages of the degradation–regeneration process. Reprinted from [120], with the permission of AIP Publishing.

reaction, as illustrated in equation (9), including hydrogen and an unknown species X, is used to explain the mechanism of LeTID. At the beginning of the degradation, hydrogen and X is forming the recombination active center HX responsible for LeTID. Later, hydrogen is continuously depleted by another reaction into H_2C , and therefore the reversible reaction turns back to the recombination inactive X, which is corresponding to the regeneration process:



In gallium doped crystalline silicon, LeTID also exists but the mechanism is different. In literature, Winter *et al* [114] reported that gallium doped crystalline silicon exhibited different degradation time constant with B-doped FZ silicon, but the calculated activation energies for both materials were in the narrow range of $(0.58 \pm 0.04)\text{ eV}$. Table 2 lists a collection of reported activation energies of degradation and regeneration processes in LeTID induced by different treatments and for diverse silicon materials. These data not only demonstrates that LeTID can affect almost all kinds of silicon materials but also provides some insight of potential participants of LeTID. Furthermore, it is worth noting that there are some differences among these values, which is probably caused by the influence from other crystallographic defects in these materials. It is also found in the paper that the degradation in gallium doped crystalline silicon is triggered by the fast-firing process when the hydrogen rich passivation layers are present, which suggestss that hydrogen is likely be involved in the LeTID formation in gallium doped silicon. Furthermore, Kwaplil *et al* [72] reported that the defect in degraded gallium doped silicon had a capture cross sectional ratio of approximately 26, which is typical for the LeTID defect. Besides, Grant *et al* [115] found that dark annealing can have a significant impact on the degradation kinetics of gallium doped crystalline silicon. In detail, after dark annealing, the previously stabilized gallium

Table 2. List of literature-reported activation energies of the degradation and regeneration processes in LeTID induced by different treatments on various silicon materials.

Source	Sample type	Treatment	Activation energies (eV)	
			Degradation	Regeneration
Winter <i>et al</i> [114]	B-doped Fz-Si wafers	1 sun illumination	0.57 ± 0.02	None
	Ga-doped Cz-Si wafers		0.58 ± 0.04	
Bredemeier <i>et al</i> [116]	B-doped mc-Si wafers	0.5 suns illumination	$E_{\text{fast}} = 0.89 \pm 0.04$	None
			$E_{\text{slow}} = 0.94 \pm 0.06$	
Vargas <i>et al</i> [117]	B-doped mc-Si wafers	Dark anneal	1.08 ± 0.05	1.11 ± 0.04
Hu <i>et al</i> [118]	B-doped cm-Si PERC cells	1.3 suns illumination	0.828 ± 0.013	1.179 ± 0.070
		12 A current injection	0.790 ± 0.064	1.059 ± 0.112
Zhou <i>et al</i> [119]	B-Ga co-doped cm-Si wafers	7 suns illumination	0.65 ± 0.05	0.80 ± 0.04
Liu <i>et al</i> [120]	P-type mc-Si wafers	$14.6 \sim 74.5 \text{ kW m}^{-2}$ illumination	$0.62 \sim 0.78$	$0.67 \sim 0.78$
Lin <i>et al</i> [37]	Ga-doped Cz-Si wafers	0.7 suns illumination	$E_{\text{fast}} = 0.96 \pm 0.04$	0.92 ± 0.03
			$E_{\text{slow}} = 0.90 \pm 0.05$	
Chen <i>et al</i> [113]	N-type Cz-Si wafers	Dark anneal	$E_{\text{slow}} = 0.76 \pm 0.02$	0.97 ± 0.01
		0.02 kW m^{-2} illumination	$E_{\text{fast}} = 0.30 \pm 0.1$	
			$E_{\text{slow}} = 0.70 \pm 0.05$	0.83 ± 0.15
			$E_{\text{SRD}} = 0.38 \pm 0.1$	

doped PERC devices underwent a fast degradation followed by a complete recovery, characteristic of LeTID, indicating that the low-temperature dark anneal has undone the effects of stabilization. Overall, the LeTID in gallium doped crystalline silicon also needs the participation of hydrogen, but the kinetics are different with the LeTID in boron-doped crystalline silicon, which might be due to the different binding energies of H–B or H–Ga complexes [72].

In summary, LeTID is a common carrier injection induced degradation phenomenon in crystalline silicon. Up to date, the exact defect responsible for LeTID is still unknown. Nevertheless, hydrogen is confirmed, by many researchers, to participate in the formation of LeTID. There are many hypotheses to explain the role of hydrogen in LeTID formation. Among them, interstitial hydrogen bonding with an unknown species X to form a recombination active complex is typically considered as a possible mechanism and H–B or H–Ga pairs are confirmed to be the hydrogen source for interstitial hydrogen.

4. Huge benefits of hydrogenation on next-generation silicon solar cells

Next generation silicon solar cells such as TOPCon and SHJ have received intense interest from photovoltaic industry and research institutes, as they have a much higher efficiency limit up to 28.7% as compared to 24.5% for PERC solar cells [121]. As TOPCon and SHJ solar cells typically have much better surface passivation via the use of passivating contact technique, the bulk lifetime of the silicon wafer becomes increasingly important for obtaining high efficiency in next generation silicon solar cells. Up to date, the cell manufacturers typically use n-type Czochralski (Cz) silicon wafer as the substrate for next-generation silicon solar cells, as Cz silicon wafer is relatively cheap and n-type silicon wafer is less sensitive to metallic impurities. Nevertheless, n-type Cz-Si wafer still suffers from the defects such as oxygen precipitates

and thermal donors. Fortunately, hydrogen is able to passivate oxygen precipitates and thermal donors and therefore is an effective way to improve the bulk lifetime of n-type Cz silicon wafer.

The typical defects in n-type Cz silicon, like oxygen precipitates, thermal donors and metallic impurities, can be well passivated by hydrogen. In terms of oxygen precipitates, Koizuka *et al* [122] reported that oxygen precipitates in n-type Cz silicon can induce two defect energy levels at about $E_c - 0.25 \text{ eV}$ and $E_v + 0.3 \text{ eV}$. Furthermore, hydrogen can passivate the oxygen precipitates by reducing the defect density at the above two energy levels. In addition, Hallam *et al* [123] found that oxygen precipitates emerged as a ring-like pattern in photoluminescence image and could reduce the efficiency of the cell up to 5% absolute. Advanced hydrogenation technique is found to completely passivate oxygen precipitates with no evident recombination activity present after passivation and in the complete solar cells, as shown in figure 24. When the oxygen precipitates are contaminated with impurity, the case is more complex. For instance, Li *et al* [124] demonstrated that iron contamination can enhance the number of oxygen precipitates in silicon, but reduce the size of them. Besides, from the results of EBIC test, the oxygen precipitates without iron contamination have a shallow defect energy level, whereas the oxygen precipitates with iron contamination have a deep defect energy level. Nevertheless, hydrogen is able to passivate the oxygen precipitates both with and without iron contamination, although the effect is better for the contaminated one, as shown in figure 25.

Hydrogen is also able to passivate thermal donors. For instance, Johnson *et al* [125] reported that the concentration of thermal donors in n-type silicon can be reduced by hydrogenation by a factor of 4.5, as shown by the DLTS result in figure 26. Nevertheless, Rashkeev *et al* [126] found that although hydrogen can passivate the thermal donors, the passivation effect is incomplete with a sizeable number of electrically active thermal donors still remaining in the sample

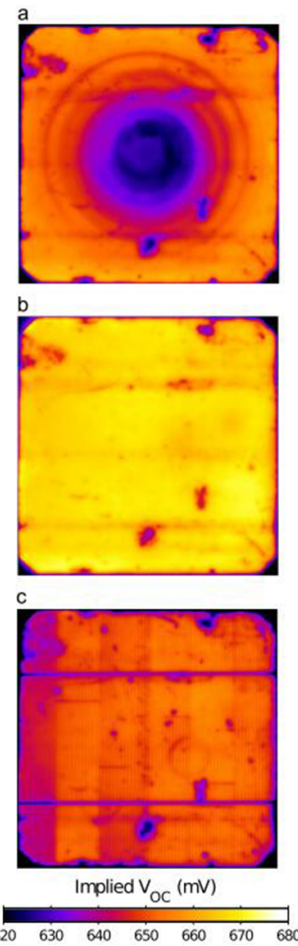


Figure 24. Calibrated 1-sun implied open circuit voltage images of a boron-doped Cz-Si wafer containing oxygen precipitates after (a) the deposition of $\text{SiN}_x:\text{H}$, (b) after an advanced hydrogenation process, and (c) on the finished device. The batch consisted of 20 wafers with 10% showing the presence of oxygen precipitate related recombination after emitter diffusion/oxidation. All wafers with oxygen precipitates were free of such recombination centers after hydrogenation. Reprinted from [132], Copyright (2015), with permission from Elsevier. Please note that implied open circuit voltage image is a collection of implied open circuit voltage value for each pixel. More information about implied open circuit voltage image can be found in [123].

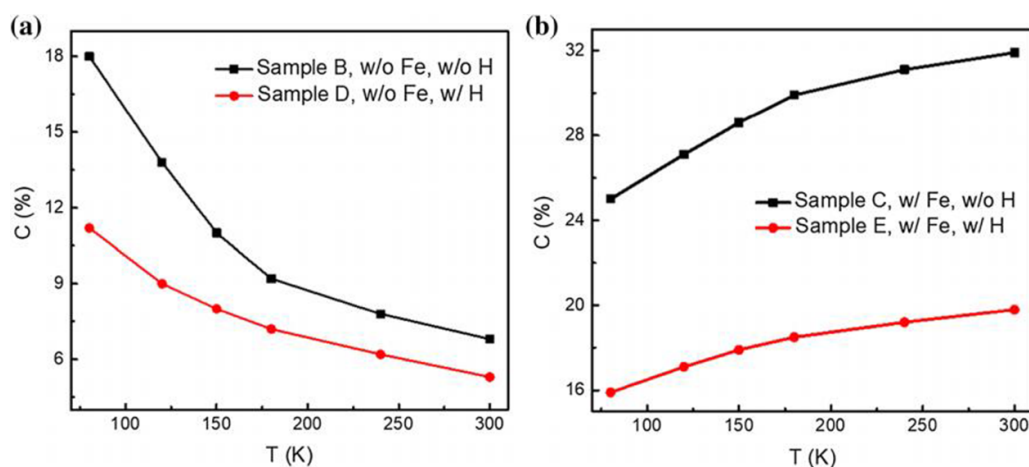


Figure 25. Temperature dependence of EBIC contrast for different samples before and after hydrogenation. (a) Samples without Fe contamination, and (b) samples with Fe contamination. Reproduced from [133], with permission from Springer Nature.

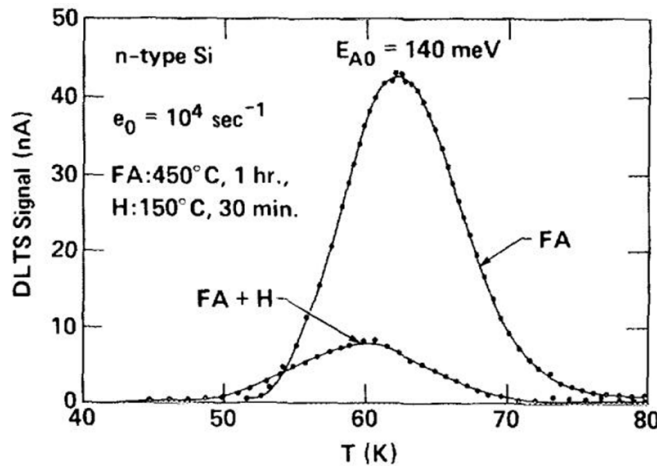


Figure 26. Effect of hydrogenation on the DLTS spectrum of the thermal-donor defect in phosphorus-doped silicon. A furnace anneal (FA) at 450 °C for 1 h generated thermal-donor defects. Hydrogenation (H, hydrogen plasma, 150 °C, 30 min) reduced the concentration of thermal donors. Reprinted from [134], with the permission of AIP Publishing.

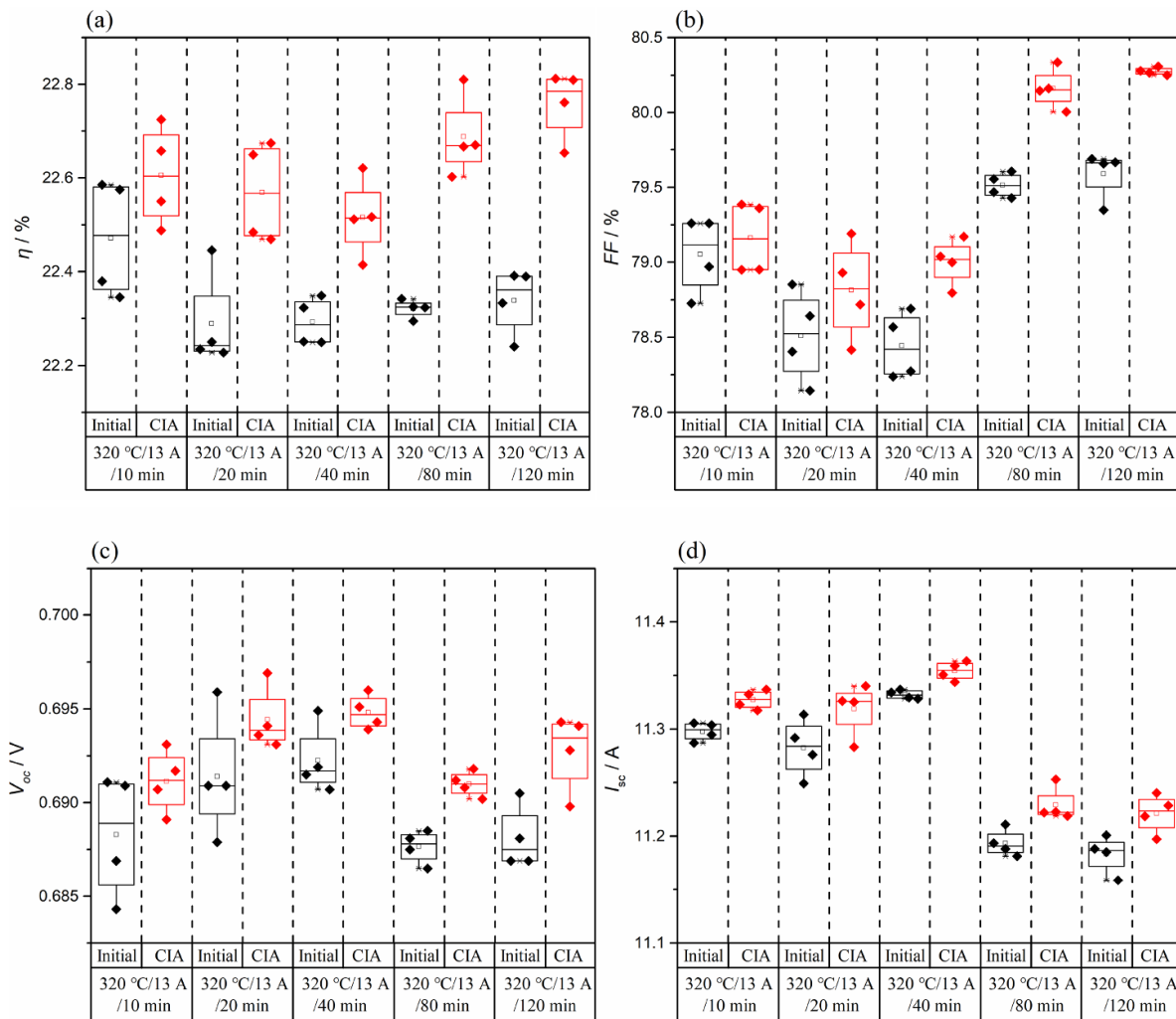


Figure 27. The changes in (a) conversion efficiency, (b) fill factor, (c) open circuit voltage, (d) short circuit current before and after 13 A current injection at 320 °C with different CIA duration (10, 20, 40, 80 and 120 min), respectively. [138] John Wiley & Sons. © 2022 WILEY-VCH Verlag GmbH & Co. KGaA, Weinheim.

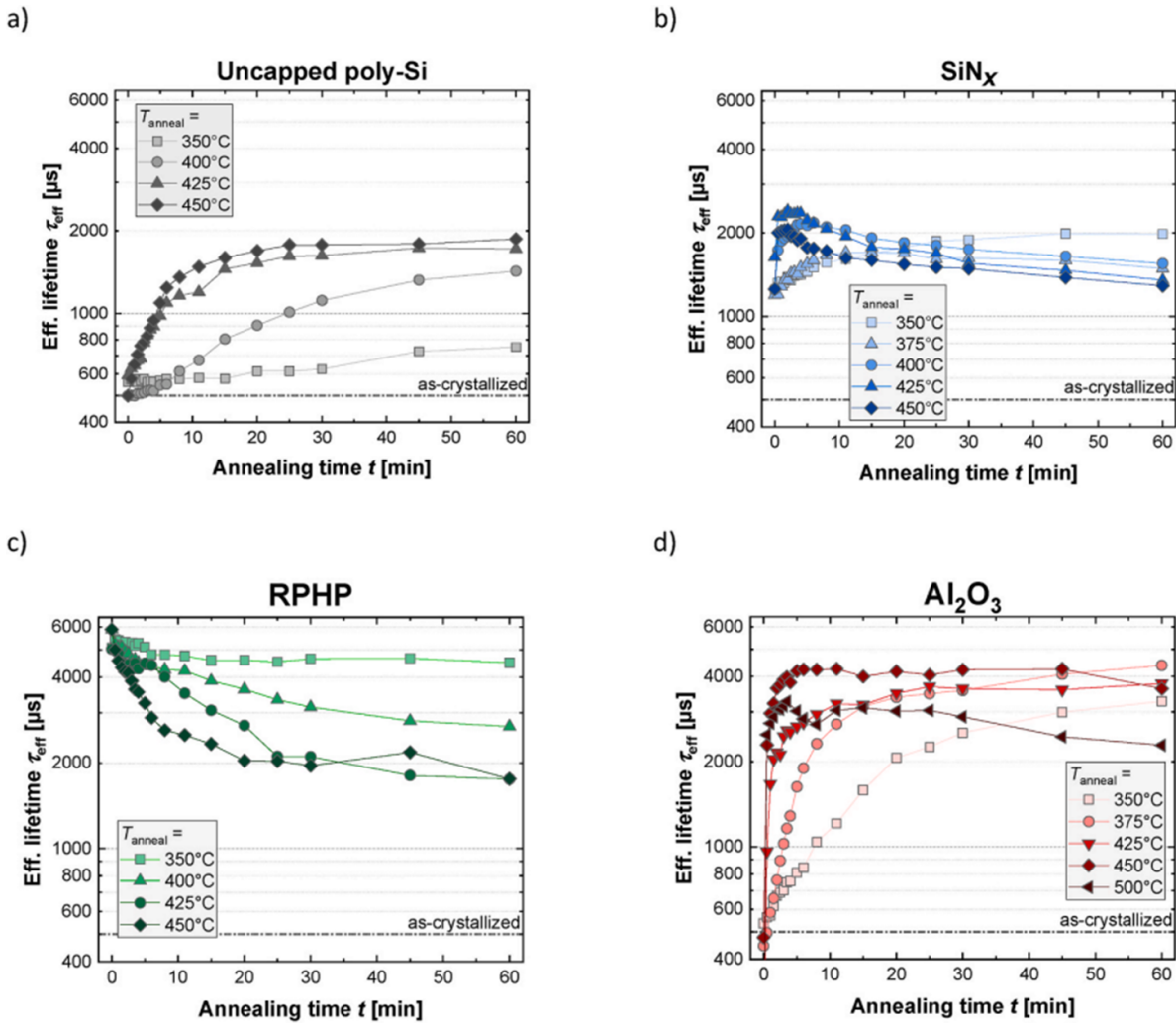


Figure 28. Effective lifetime of n-type TOPCon samples on textured surface after hotplate annealing with different hydrogen sources: (a) uncapped poly-Si, (b) SiN_x , (c) remote hydrogen plasma treatment and (d) Al_2O_3 . Reprinted from [132], Copyright (2021), with permission from Elsevier.

after hydrogenation. The reason might be that the hydrogenation of thermal donors in crystalline silicon is a reversible reaction.

Although n-type silicon is insensitive to the typical metallic impurity like Fe, some metallic impurities like Ti, Cr, and Ni even show severer recombination activity in n-type silicon. Fortunately, hydrogen is still able to passivate these metallic impurities like Ti. In detail, Leonard *et al* [127] reported that a room-temperature hydrogen plasma has resulted in the suppression of DLTS signals due to interstitial Ti atoms and the appearance of three strong DLTS peaks, which are related to three different Ti-H complexes. Then after annealing of the hydrogenated samples at 150 °C in nitrogen, the signals due to interstitial Ti and two of the three Ti-H complexes were not detected in the spectra showing that almost complete passivation of all the electrically active defects occurred. The information on hydrogen passivation of Cr and Ni in n-type silicon is discussed in section 3.2.

Moreover, the enhanced passivation of interface defects is also the challenging issue in order to further improve the electrical performance of TOPCon and SHJ solar cells.

For instance, Yang *et al* [130] found that the effective carrier lifetime of the n-Si/tunnel oxide/poly-Si structure can be enhanced during illumination at elevated temperature only when $\text{SiN}_x:\text{H}$ coating is present. Besides, by measuring the change of J_0 during the carrier-induced hydrogenation treatment, they proposed that hydrogen is of significance in the enhanced Si/SiO_x interface defects passivation. More recently, Hu *et al* [128] also reported the improved conversion efficiency of TOPCon solar cells by using current injection and annealing (CIA) treatment, as shown in figure 27, which could also be related to the enhanced hydrogenation of interface defects. For details, the change in the electrical properties of Si/SiO₂ interface after hydrogenation has been discussed in [129]. Furthermore, Polzin *et al* [131] compared hydrogenation of Si/SiO_x interface defects in poly-Si based passivating contact structures with different hydrogen sources by using different capping layers, as the evolution of effective lifetime during annealing given in figure 28. Their results also confirmed the increased interface passivation quality after thermal annealing with the participation of hydrogen.

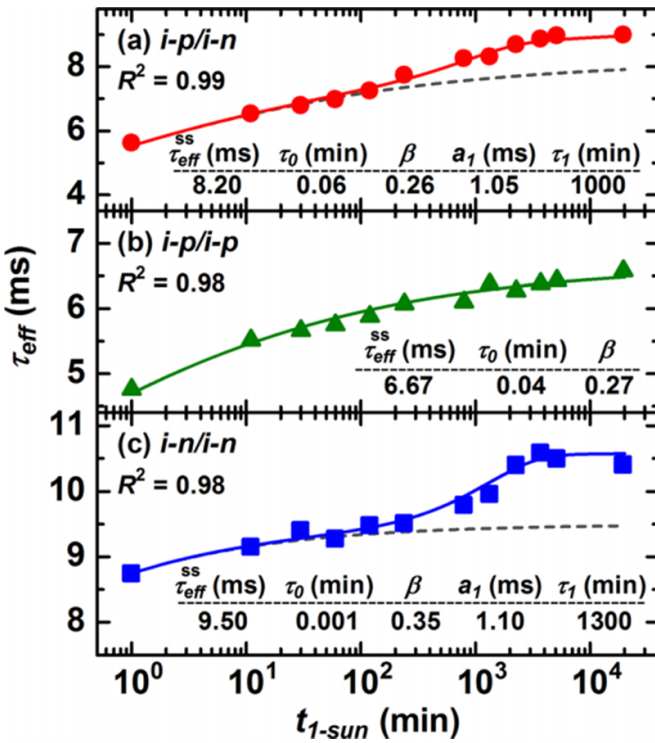


Figure 29. Measured values for τ_{eff} as function of $t_{1\text{-sun}}$. Symbols represent measured data, whereas solid lines show (a) and (c) power law and field effect fits and (b) power law to the data. Dashed lines show the part of the power law only. Values for the fitting parameters are given in the inset table. Reprinted from [138], with the permission of AIP Publishing.

As for SHJ solar cells, a structure of c-Si coated with doped/intrinsic a-Si:H bilayers exactly is the key component of SHJ solar cells, since the hydrogenated i-a-Si layers between the c-Si bulk and the doped a-Si:H can efficiently passivate the interface dangling bonds [132]. Hydrogen engineering in order to improve the performance of SHJ solar cells has been widely studied, for instance, Soman *et al* [133] reported that hydrogen plasma with annealing as post-treatments for SHJ solar cells leads to decreased reverse saturation current, which could be attributed to the interface defects passivation, they also investigated the relation between the hydrogen plasma properties to the passivation quality of c-Si surface [134]. Besides, Liu *et al* [135] found that the post H₂ plasma treatment with residual SiH₄ molecules contributes to the formation of a dense silicon layer which can inhibit the out diffusion of hydrogen from bulk, thus, causing evident enhancement in the J_{sc} , V_{oc} and E_{ff} of SHJ solar cells. Xu *et al* [136] also demonstrated that microwave H₂ plasma treatment before a-Si:H deposition can effectively reduce surface recombination velocity as low as 4 cm s⁻¹.

The phenomenon of light induced performance increase was also observed in SHJ solar cells, with the efficiency gain of about 0.3%_{abs} [137], as shown in figure 29. They referred the improvement is related to the enhanced surface passivation quality i.e. the reduction in the recombination active interface defect density, furthermore, the improvement requires the presence of the doped a-Si:H layers. The light

induced performance increase in SHJ solar cells has been also reported by Wright *et al* [36], and Bao *et al* [138] more recently. These experiments confirmed that the light soaking and annealing can efficiently enhance the conversion efficiency of SHJ solar cells with different initial efficiency and from different production lines, which could be valuable for the global PV industry.

5. Conclusions

At the beginning, the fundamental properties of hydrogen in crystalline silicon are reviewed, including the diverse forms of hydrogen in silicon, the charge states of hydrogen, the hydrogen solubility, the hydrogen diffusivity and the hydrogen source. The important findings are concluded as follows. First, hydrogen can dominantly exist in four forms in crystalline silicon, namely hydrogen platelet, hydrogen dimer, interstitial hydrogen and hydrogen bound state. These forms of hydrogen have distinct electrical properties and may interact with different defects. Among these four forms of hydrogen, interstitial hydrogen is the most significant to hydrogenation as it is chemically active to passivate defects. Second, interstitial hydrogen has three charge states: H⁺, H⁻ and H⁰. The fractional concentrations of these charge states depend on the position of Fermi level in silicon bandgap. In addition, it is worth noting that different charge states of hydrogen have distinct electrical properties and manipulation of these charge states is reported to enhance the performance of hydrogenation dramatically. Third, the diffusivity of hydrogen can be influenced by temperature, electric field, the interactions with dopants and etc. At high temperature regime, hydrogen diffusivity is determined by the diffusivity of interstitial hydrogen without any trap. At modest temperature regime, hydrogen still dominantly diffuse in the form of interstitial hydrogen, but its diffusivity is significantly reduced by the interactions with dopants. At low temperature regime, the diffusivity of hydrogen is determined by the diffusivity of hydrogen dimers, which are very slow. Fourth, the hydrogenated silicon nitride film (SiN_x:H) is typically used as the hydrogen source for silicon solar cells. Generally, the refractive index of the SiN_x:H film can be modulated to vary the amount of atomic hydrogen into silicon bulk and this value need to be experimentally adjusted to give better hydrogenation effect. Firing temperature also plays an important role on the amount of hydrogen released from the SiN_x:H film and typically 750 °C will be best for hydrogen in-diffusion to silicon bulk.

Then, the applications of hydrogenation on diverse defects in crystalline silicon are discussed in section 3, with the emphasis on passivation kinetics and mechanism. First, dopant passivation by hydrogen is a well-known phenomenon, and it is found that the neutralization of dopant requires an oppositely charged hydrogen to form complex. Nevertheless, the dopant-hydrogen complex is not stable and can dissociate at elevated temperatures and under carrier injection. Second, hydrogen is able to passivate most of typical metallic impurities in crystalline silicon. However, the passivation mechanisms for each metallic impurity is different. Generally,

it is found that the metallic impurity-H₁ complex still has some recombination activity, but with more hydrogen atoms attaching to the metallic impurity, the complex becomes inactive. Third, hydrogen is also able to passivate dislocations and grain boundaries, however, the passivation effectiveness depends on the character of GB and the contamination level. Furthermore, three important assumptions are concluded for explaining the mechanism of hydrogenation on grain boundaries. Fourth, hydrogen is able to passivate silicon surface states both with and without contamination. For clean silicon surface, hydrogenation can reduce the density of silicon surface states to several folds smaller. For contaminated silicon surface, hydrogenation can result in the agglomeration of the two-dimensional metal layers into the three-dimensional metal islands. Fifth, the regeneration process of B–O related defects requires hydrogen to participate in and the detailed mechanism is found to be hydrogen bonding with B–O related defects to form a recombination inactive complex. Moreover, recent works indicated that H⁰ is directly responsible for the regeneration process and therefore carrier injection such as laser illumination can dramatically enhance the rate of the regeneration process. Sixth, hydrogen typically is a passivation species to deactivate defects, however, hydrogen becomes a species to induce defect in the case of LeTID. Strong evidences are found to prove that hydrogen is necessary for the formation of LeTID in crystalline silicon. There are many hypotheses to explain the role of hydrogen in LeTID formation. Among them, interstitial hydrogen bonding with an unknown species X to form a recombination active complex is typically considered as a possible mechanism and H–B pairs are confirmed to be the hydrogen source for interstitial hydrogen.

At last, the benefits of hydrogenation on next-generation silicon solar cells are reviewed. In detail, hydrogenation can improve the conversion efficiency of TOPCon and SHJ solar cells by more than 0.2% absolute. The mechanism of this improvement lies on the hydrogenation of the defects, including the bulk defects such as oxygen precipitate, thermal donor and some metallic impurities, and the interface defects around the Si/SiO_x and Si/a-Si interface. Fortunately, hydrogen can well passivate these defects and make them recombination inactive after hydrogenation, which will lead to the further improvement of the electrical performance in these solar cells.

Future research may focus more on the microscopic mechanism of hydrogenation on typical defects in crystalline silicon and find out the chemical compositions and configurations of the hydrogen-defect complexes.

Data availability statement

The data that support the findings of this study are available upon reasonable request from the authors.

Acknowledgments

The authors would like to thank National Natural Science Foundation of China (Nos. 62025403, 61974129, 61721005 and 62004173), Visiting Scholars Foundation of State Key

Laboratory of Silicon Materials (SKL2020-01), Natural Science Foundation of Zhejiang Province (D22E028801) ‘Pioneer’ and ‘Leading Goose’ R&D Program of Zhejiang (No. 2022C01215), and the Fundamental Research Funds for the Central Universities (226-2022-00200) for financial support.

ORCID iDs

Lihui Song  <https://orcid.org/0000-0001-5536-8388>
 Zechen Hu  <https://orcid.org/0000-0002-8203-3089>
 Xuegong Yu  <https://orcid.org/0000-0002-0354-8501>

References

- [1] Wang A, Zhao J and Green M A 1990 *Appl. Phys. Lett.* **57** 602–4
- [2] Feldmann F, Bivour M, Reichel C, Hermle M and Glunz S W 2014 *Sol. Energy Mater. Sol. Cells* **120** 270–4
- [3] Tanaka M, Taguchi M, Matsuyama T, Sawada T, Tsuda S, Nakano S, Hanafusa H and Kuwano Y 1992 *Jpn. J. Appl. Phys.* **31** 3518–22
- [4] Feldmann F, Bivour M, Reichel C, Steinkemper H, Hermle M and Glunz S W 2014 *Sol. Energy Mater. Sol. Cells* **131** 46–50
- [5] Wu Z, Zhang L, Chen R, Liu W, Li Z, Meng F and Liu Z 2019 *Appl. Surf. Sci.* **475** 504–9
- [6] Descoedres A *et al* 2011 *Appl. Phys. Lett.* **99** 18
- [7] Binns M J, Newman R C, Mcquaid S A and Lightowers E C 1993 *Mater. Sci. Forum* **143–147** 861–6
- [8] Wieringen A V and Warmoltz N 1956 *Physica* **22** 849–65
- [9] Pearton S J, Chantre A M, Kimerling L C, Cummings K D and Dautremont-Smith W C 1985 *MRS Proc.* **59** 475
- [10] Newman R C, Tucker J H, Brown A R and Mcquaid S A 1991 *J. Appl. Phys.* **70** 3061–70
- [11] Mathiot D 1989 *Phys. Rev. B* **40** 5867–70
- [12] Pantelides S T 1986 *Mater. Sci. Forum* **10–12** 573–8
- [13] Denteneer P J H, Walle C G V D, Bar-Yam Y and Pantelides S T 1989 *Mater. Sci. Forum* **38–41** 979–84
- [14] Johnson N M and Herring C 1991 *Proc. Mater. Sci. Forum* **38–41** 961–6
- [15] Herring C, Johnson N M and Van de Walle C G 2001 *Phys. Rev. B* **64** 125209
- [16] Kamiura Y 2003 *Strateg. Manage. J.* **30** 1–23
- [17] Liu A Y, Sun C and Macdonald D 2014 *J. Appl. Phys.* **116** 194902–10
- [18] Hallam B J, Wenham S R, Hamer P G, Abbott M D, Sugianto A, Chan C E, Wenham A M, Eadie M G and Xu G Q 2013 *Energy Proc.* **38** 561–70
- [19] Streicher S 1987 *Phys. Rev. B* **36** 9122
- [20] Chang K J and Chadi D J 1988 *Phys. Rev. Lett.* **60** 1422
- [21] Martinuzzi S, Périchaud I and Warchol F 2003 *Sol. Energy Mater. Sol. Cells* **80** 343–53
- [22] Ciesla A M, Chan C E, Wang S, Abbott M D, Chong C M and Wenham S R 2018 *Proc. 2017 IEEE 44th Photovoltaic Specialist Conf. (PVSC)*
- [23] Bardhadi A, Amzil H, Muller J C and Siffert P 1989 *Polycrystalline semiconductors* (Berlin: Springer)
- [24] Park Y, Lu J and Rozgonyi G 2009 *J. Appl. Phys.* **105** 6247
- [25] Jiang T, Yu X, Gu X, Yang D and Rozgonyi G 2012 *Phys. Status Solidi a* **209** 990–3
- [26] Jones R, Öberg S, Goss J, Briddon P R and Resende A 2015 *Phys. Rev. Lett.* **75** 2734–7
- [27] Latham C D, Alatalo M, Nieminen R M, Jones R, Berg S and Briddon P R 2005 *Phys. Rev. B* **72** 235205
- [28] Nampalli N, Hallam B J, Chan C E, Abbott M D and Wenham S R 2015 *IEEE J. Photovolt.* **5** 1580–5

- [29] Wilking S, Beckh C, Ebert S, Herguth A and Hahn G 2014 *Sol. Energy Mater. Sol. Cells* **131** 2–8
- [30] Lin D, Hu Z, He Q, Yang D, Yu X and Yu X 2021 *Sol. Energy Mater. Sol. Cells* **226** 111085
- [31] Chan C, Hamer P, Bourret-Sicotte G, Ran C, Ciesla A, Hallam B, Payne D, Bonilla R S, Wenham S and Chan C 2017 *Sol. RRL* **1** 1700129
- [32] Ciesla A *et al* 2018 *Prog. Photovolt.* **26** 2986
- [33] Liu C, Chen D, Chen Y, Ling Y, Zou Y, Wang Y, Gong J, Feng Z, Altermatt P P and Verlinden P J 2020 *Sol. Energy Mater. Sol. Cells* **215** 110690
- [34] Madumelu C, Wright B, Soeriyadi A, Wright M, Chen D, Hoex B and Hallam B 2020 *Sol. Energy Mater. Sol. Cells* **218** 110752
- [35] Wright M *et al* 2021 *Phys. Status Solidi* **15** 2100170
- [36] Wright M, Kim M, Dexiang P, Xin X and Hallam B 2019 *Proc. 15th Int. Conf. on Concentrator Photovoltaic Systems (CPV-15)*
- [37] Lin D, Hu Z, Song L, Yang D and Yu X 2021 *Sol. Energy* **225** 407–11
- [38] Johnson M N, Biegelsen D K and Moyer M D 1982 *Appl. Phys. Lett.* **40** 882–4
- [39] Voronkov V V and Falster R 2017 *Phys. Status Solidi c* **254** 1600779
- [40] Nickel N H, Anderson G B, Johnson N M and Walker J 2000 *Phys. Rev. B* **62** 8012–5
- [41] Sopori B, Zhang Y, Reedy R, Jones K, Yan Y, Al-Jassim M, Bathey B and Kalejs J 2005 *Proc. IEEE Photovoltaic Specialists Conf.*
- [42] Sun C, Rougier F E and Macdonald D 2015 *J. Appl. Phys.* **117** 153–372
- [43] Hallam B J, Hamer P G, Wenham A M C N, Chan C E, Stefani B V and Wenham S 2020 *Prog. Photovolt.* **28** 1217–38
- [44] Hallam B, Abbott M, Nampalli N, Hamer P and Wenham S 2016 *J. Appl. Phys.* **119** 404
- [45] McQuaid S A, Binns M J, Newman R C, Lightowers E C and Clegg J B 1993 *Appl. Phys. Lett.* **62** 1612–4
- [46] Song L 2016 *Appl. Phys. A* **122** 930
- [47] Saad A M, Velichko O, Shaman Y P, Barcz A, Misiuk A and Fedotov A K 2008 *Solid State Phenom.* **131–133** 425–30
- [48] Kamiura Y, Yoneta M and Hashimoto F 1991 *Appl. Phys. Lett.* **59** 3165–7
- [49] Johnson N M and Herring C 1992 *Phys. Rev. B* **46** 15554–7
- [50] Dautremont-Smith W C, Nabity J C, Swaminathan V, Stavola M, Chevallier J, Tu C W and Pearton S J 1986 *Appl. Phys. Lett.* **49** 1098–100
- [51] Muller J C, Ababou Y, Barhdadi A, Courcelle E, Unamuno S, Salles D, Siffert P and Fally J 1986 *Sol. Cells* **17** 201–31
- [52] Dhungel S K, Yoo J, Kim K, Karunagaran B, Sunwoo H, Mangalaraj D and Yi J 2004 *Mater. Sci. Semicond. Process.* **7** 427–31
- [53] Fenner D B, Biegelsen D K and Bringans R D 1989 *J. Appl. Phys.* **66** 419–24
- [54] Trucks G W, Raghavachari K, Higashi G S and Chabal Y J 1990 *Phys. Rev. Lett.* **65** 504
- [55] W. A., Lanford M and Rand J 1978 *J. Appl. Phys.* **49** 2473–7
- [56] Barakel D, Ulyashin A, Périchaud I and Martinuzzi S 2002 *Sol. Energy Mater. Sol. Cells* **72** 285–90
- [57] Lee S H, Bhopal M F, Lee D W and Lee S H 2018 *Mater. Sci. Semicond. Process.* **79** 66–73
- [58] Anthony B 1989 *J. Vac. Sci. Technol. B* **7** 621–6
- [59] Lelièvre J F, Fourmond E, Kaminski A, Palais O, Ballutaud D and Lemiti M 2009 *Sol. Energy Mater. Sol. Cells* **93** 1281–9
- [60] Hong J, Kessels W M M, Soppe W J, Weeber A W, Arnoldbik W M and van de Sanden M C M 2003 *J. Vac. Sci. Technol. B* **21** 2123–32
- [61] Dekkers H F W, Beaucarne G, Hiller M, Charifi H and Slaoui A 2006 *Appl. Phys. Lett.* **89** 073516
- [62] Liu J, Hamada K, Akagi S, Ooyagi N, Ohdaira K and Ohdaira K 2020 *Surf. Interfaces* **21** 100690
- [63] Brett H, Tjahjono B and Wenham S 2012 *Sol. Energy Mater. Sol. Cells* **96** 173–9
- [64] Chen F, Romijn I, Weeber A, Tan J, Hallam B and Cotter J 2007 *22nd European Photovoltaic Solar Energy Conf. and Exhibition*
- [65] Sveinbjörnsson E and Engström O 1995 *Phys. Rev. B* **52** 4884–95
- [66] Yarykin N, Sachse J U, Lemke H and Weber J 1999 *Phys. Rev. B* **59** 5551–60
- [67] Yelundur V, Rohatgi A, Jeong J W, Gabor A M, Hanoka J I and Wallace R L 2000 *Conference Record of the Twenty-Eighth IEEE Photovoltaic Specialists Conference* vol 30 pp 91–94
- [68] Hameiri Z, Mai L, Borojevic N, Javid S, Tjahjono B S, Sugianto A, Wang S, Sprout A B and Wenham S R 2009 *Proc. Int. Photovoltaic Science and Engineering Conf.*
- [69] Song L, Zheng X, Fu J and Ji Z 2017 *J. Alloys Compd.* **698** 892–7
- [70] Chang K J and Chadi D J 1989 *Phys. Rev. B* **40** 11644–53
- [71] Zundel T and Weber J 1991 *Phys. Rev. B* **43** 4361–72
- [72] Kwapisz W, Dalke J, Post R and Niewelt T 2021 *Sol. RRL* **5** 2100147
- [73] Pickett M and Buonassisi T 2008 *Appl. Phys. Lett.* **92** 489
- [74] Davis R J Jr., Rohatgi A, Hopkins H R, Blais P D, Rai-Choudhury P, McCormick J R and Mollenkopf H C 1980 *IEEE Trans. Electron Devices* **27** 677–87
- [75] Liu A Y, Sun C, Markevich V P, Peaker A R, Murphy J D and Macdonald D 2016 *J. Appl. Phys.* **120** 489–534
- [76] Leonard S, Markevich V P, Peaker A R, Hamilton B and Murphy J D 2015 *Appl. Phys. Lett.* **68** 13
- [77] Sadoh T *et al* 1997 *J. Appl. Phys.* **82** 3828–31
- [78] Knack S, Weber J, Lemke H and Riemann H 1999 *Phys. B* **273–274** 387–90
- [79] Sachse J U, Sveinbjörnsson E, Jost W, Weber J and Lemke H 1997 *Phys. Rev. B* **55** 16176–85
- [80] Song A W L *et al* 2015 *Int. J. Photoenergy* **2015** 1–13
- [81] Dube C and Hanoka J I 1984 *Appl. Phys. Lett.* **45** 1135–7
- [82] Glaenzner R H and Jordan A G 1969 *Solid State Electron.* **12** 247–58
- [83] Kveder V, Kittler M and Schröter W 2001 *Phys. Rev. B* **63** 115208
- [84] Sopori B 2002 *J. Electron. Mater.* **31** 972–80
- [85] Divigalpitiya W M R, Morrison S R and Vercruyssse G 1987 *Sol. Energy Mater.* **15** 141–51
- [86] Weronek K, Weber J and Queisser H J 1993 *Phys. Status Solidi a* **137** 543–8
- [87] Kittler M, Seifert W and Knobloch K 2003 *Microelectron. Eng.* **66** 281–8
- [88] Rinio M, Kaes M, Hahn G and Borchert D 2006 *Twentyfirst European Photovoltaic Solar Energy Conference (Gelsenkirchen, Germany)* vol 2
- [89] Mao X, Yu X, Yuan S and Yang D 2019 *Appl. Phys. Express* **12** 051012
- [90] Chen J, Yang D, Xi Z and Sekiguchi T 2005 *Physica B* **364** 162–9
- [91] Maydell K V and Nickel N H 2007 *Appl. Phys. Lett.* **90** 3285
- [92] Bertoni M I *et al* 2015 *Prog. Photovolt.* **19** 187–91
- [93] Yu X, Li X, Lei D, Yang D and Rozgonyi G 2011 *Scr. Mater.* **64** 653–6
- [94] Leguijt C, Lötgen P, Eikelboom J A, Weeber A W, Schuurmans F M, Sinke W C, Alkemade P F A, Sarro P M, Marée C H M and Verhoef L A 1996 *Sol. Energy Mater. Sol. Cells* **40** 297–345

- [95] Walle V D and Chris G 1998 *J. Vac. Sci. Technol. A* **16** 1767–71
- [96] Cartier E, Buchanan D A and Dunn G J 1994 *Appl. Phys. Lett.* **64** 901–3
- [97] Oura K, Lifshits V G, Saranin A A, Zотов A V and Katayama M 2016 *Surf. Sci. Rep.* **35** 1–69
- [98] Bothe K, Hezel R and Schmidt J 2003 *Appl. Phys. Lett.* **83** 1125–7
- [99] Hallam B, Kim M, Abbott M, Nampalli N, Nærland T, Wenham S, Stefani B and Wenham S 2017 *Sol. Energy Mater. Sol. Cells* **173** 25–32
- [100] Wilking S, Herguth A and Hahn G 2013 *Energy Proc.* **38** 642–8
- [101] Schmidt J and Bothe K 2004 *Phys. Rev. B* **69** 1129–33
- [102] Herguth A, Schubert G, Kaes M and Hahn G 2008 *Prog. Photovolt.* **16** 135–40
- [103] Hallam B, Hamer P, Kim M, Nampalli N and Wenham S 2016 *Proc. Photovoltaic Specialists Conf.*
- [104] Walter D C, Lim B, Bothe K, Voronkov V V, Falster R and Schmidt J 2014 *Appl. Phys. Lett.* **104** 404–289
- [105] Niewelt T, Schön J, Warta W, Glunz S W and Schubert M C 2017 *IEEE J. Photovolt.* **7** 383–98
- [106] Herguth A and Hahn G 2010 *J. Appl. Phys.* **108** 325
- [107] Bredemeier D, Walter D, Herlufsen S and Schmidt J 2016 *AIP Adv.* **6** 035119
- [108] Chan C E, Payne D N R, Hallam B J, Abbott M D, Fung T H, Wenham A M, Tjahjono B H and Wenham S R 2016 *IEEE J. Photovolt.* **6** 1473–9
- [109] Schmidt J, Bredemeier D and Walter D C 2019 *IEEE J. Photovolt.* **9** 1497–503
- [110] Chan C, Fung T H, Abbott M, Payne D, Wenham A, Hallam B, Chen R and Wenham S 2017 *Sol. RRL* **1** 1600028
- [111] Jensen M A, Zuschlag A, Wieghold S, Skorka D, Morishige A E, Hahn G and Buonassisi T 2018 *J. Appl. Phys.* **124** 085701–8
- [112] Philip E M, Weiser M, Haug H, Wiig M S and Søndenå R 2020 *J. Appl. Phys.* **127** 065703
- [113] Chen D *et al* 2020 *Sol. Energy Mater. Sol. Cells* **207** 110353
- [114] Winter M, Walter D C and Schmidt J 2021 *IEEE J. Photovolt.* **11** 866–72
- [115] Grant N, Scowcroft J R, Pointon A I, Al-Amin M, Altermatt P P and Murphy J D 2020 *Sol. Energy Mater. Sol. Cells* **206** 110299
- [116] Bredemeier D, Walter D and Schmidt J 2017 *Sol. Energy Mater. Sol. Cells* **173** 2–5
- [117] Vargas C, Coletti G, Chan C, Payne D and Hameiri Z 2019 *Sol. Energy Mater. Sol. Cells* **189** 166–74
- [118] Hu Z, He Q, Yuan S, Lin D, Song L, Yu X and Yang D 2021 *Sol. RRL* **5** 2100035
- [119] Zhou C, Ji F, Cheng S, Zhu J, Wang W and Dong H 2020 *Sol. Energy Mater. Sol. Cells* **211** 110508
- [120] Liu S, Chan C, Chen D, Kim M and Payne D 2018 *Proc. SILICONPV 2018*
- [121] Jan S, Robby P and Rolf B 2018 *Sol. Energy Mater. Sol. Cells* **187** 39–54
- [122] Koizuka M and Yamada-Kaneta H 1998 *Phys. Status Solidi b* **210** 557–61
- [123] Hallam B, Chan C, Abbott M and Wenham S 2015 *Sol. Energy Mater. Sol. Cells* **141** 125–31
- [124] Li J, Song L, Yu X and Yang D 2018 *J. Electron. Mater.* **47** 5039–44
- [125] Johnson N M and Hahn S K 1986 *Appl. Phys. Lett.* **48** 709–11
- [126] Rashkeev S N, Ventra M and Pantelides S T 2001 *Appl. Phys. Lett.* **78** 1571–3
- [127] Leonard S, Markevich V P, Peaker A R and Hamilton B 2013 *Appl. Phys. Lett.* **103** 132103–4
- [128] Hu Z *et al* 2022 *Phys. Status Solidi a* **219** 2100614
- [129] Reed M L and Plummer J D 1988 *J. Appl. Phys.* **63** 5776–93
- [130] Yang Y, Altermatt P P, Cui Y, Hu Y, Chen D, Chen L, Xu G, Zhang X, Chen Y and Hamer P 2018 *AIP Conf. Proc.* **1999** 040026
- [131] Polzin J I, Hammann B, Niewelt T, Kwapił W and Feldmann F 2021 *Sol. Energy Mater. Sol. Cells* **230** 111267
- [132] Masuko K *et al* 2014 *IEEE J. Photovolt.* **4** 1433–5
- [133] Soman A, Nsofor U, Das U K, Gu T and Hegedus S S 2019 *ACS Appl. Mater. Interfaces* **11** 16181–90
- [134] Soman A, Nsofor U, Zhang L, Das U, Gu T and Hegedus S 2018 *Proc. 2017 IEEE 44th Photovoltaic Specialist Conf. (PVSC)*
- [135] Liu W, Zhang L, Cong S, Chen R, Wu Z, Meng F, Shi Q and Liu Z 2018 *Sol. Energy Mater. Sol. Cells* **174** 233–9
- [136] Xu M, Wang C, Bearda T, Simoen E, Radhakrishnan H S, Gordon I, Li W, Szlufcik J and Poortmans J 2018 *IEEE J. Photovolt.* **8** 1539–45
- [137] Kobayashi E, Wolf S D, Levrat J, Christmann G, Descoeuilles A, Nicolay S, Despeisse M, Watabe Y and Ballif C 2016 *Appl. Phys. Lett.* **109** 692
- [138] Bao S *et al* 2021 *J. Mater. Sci., Mater. Electron.* **32** 4045–52